Trends in Cancer Research
Vol. 16, 2021

Original Article

Anisotropic dose gradient measures that naturally correlate on complication rates in organs at risk

Markus Wösle*
Klinik für Strahlentherapie und Radioonkologie, Städtisches Klinikum Dessau, Dessau-Roßlau, Germany.

ABSTRACT

Dose conformity and steepness of dose fall-off at a target volume's boundary are important quality criteria in treatment planning to predict complication rates in normal tissue. The clinical validity of correlations between a dose gradient measure and treatment complications are not proved for all but one of the common dose gradient measures. The author demonstrates that more-dimensional dose gradient measures exactly describe local dose gradient distributions towards organs at risk. As a result, incidences of radiogenic toxicities in normal tissue correlate on the dose gradient measures in a natural manner. Anisotropic dose gradient problems will be described by the superficially averaged dose gradient (*SADG*). The degrees of anisotropy can be quantified by a novel geometrical metric called the relative ellipsoidality (E). The correlations between the *SADG* and dose-volume metrics for normal tissue were investigated for the linac-based stereotactic radiotherapy of 25 malignant choroidal melanomas. The ratios of the mean values of the local *SADG* to the mean value of the global *SADG* were in a range of 1.2 to 1.7. The correlation between the volume of normal tissue receiving at least 10 *Gy*, $V_{10\ Gy}$, and the global *SADG* was strong: Pearson's correlation coefficient r was 0.833 (p = 0.000). The mean dose values within the ipsilateral lacrimal glands correlated with $r \geq 0.870$ (p = 0.000) on the local *SADG*. The relative ellipsoidalities of the isodoses of interest were in a range of 1/27.3 to 1/2.1. More-dimensional dose gradient measures are urgently required for lesions that are located in non-homogeneous normal tissue. Only exact descriptions of the dose gradient distributions enable reliable prognoses of treatment complications. The parameter E is a measure of the anisotropy of dose gradient distributions and allows the estimation of the quality of dose gradient indices with respect to the description of local dose gradients and prediction of complication rates.

KEYWORDS: anisotropic dose gradient distribution, more-dimensional dose gradient measure, relative ellipsoidality of surface or volume, superficially averaged distance, superficially averaged dose gradient.

1. INTRODUCTION

Quality criteria in radiotherapy to specify the dose distribution within the target volume and at its boundary are the dose homogeneity, dose conformity, and irradiated volume. ICRU Reports no. 62 and no. 83 recommend reporting the values of these parameters [1, 2]. The dose homogeneity is a synonym for the uniformity of the dose distribution within the target volume [2]. The dose conformity characterises the degree to which the high dose region, appropriately modelled by the volume and surface of the prescribed isodose, conforms to the target volume [3]. The irradiated volume is the tissue volume that receives a dose that is considered significant in relation to normal tissue tolerance [1].

Particularly in stereotactic radiotherapy and radiosurgery, clinical complications primarily

*Email ID: markus.woesle@klinikum-dessau.de

occur due to the dose fall-off in a region between the surfaces of the prescribed isodose and another isodose with organ-specific tolerance dose levels. In this regard, good dose conformity is one of the necessary conditions for the restriction of absorbed dose to the normal tissue and organs at risk. Consequently, good dose conformity and steep dose gradients are necessary and sufficient conditions for sparing doses in healthy tissue.

The dose fall-off at the target volume's boundary can be characterised by different dose gradient measures, which are also designated as dose gradient indices or metrics in literature. Hereinafter, the author will use the terms *index* and *metric* for one-dimensional or *measure* for more-dimensional descriptions of clinical dose gradient distributions, respectively; the term *measure* will also be used if the dimension of the description is arbitrary.

ICRU Report no. 91 recommends reporting one of two simple, in other words one-dimensional, dose gradient indices in addition to a conformity index, for example, Paddick's [3, 4]: the dose gradient index (*GI*) of Paddick *et al.* [5] or the volume of normal tissue irradiated with at least the dose D, V_D, for instance, $D = 12\ Gy$ for brain tissue treated with one single-dose fraction [6, 7]. One important aim stipulated in ICRU Report no. 91 is to better associate treatment complications with the values of dose gradient indices *via* rigorous and uniform reporting of these parameters [3].

Since 2000, several one-dimensional dose gradient indices have been defined and are clinically utilised. With regard to their determination, they are based on

- single volumes of healthy tissue [6, 7],
- volume ratios of the isodoses of interest [5, 8, 9],
- the ratio of the volumes of healthy tissue under real and ideal irradiation conditions [10],
- functions of the volume product of the isodoses of interest [11],
- corrected or pure radius differences between the isodoses of interest [12-14],
- the spatially averaged dose difference quotient or radius difference between the isodoses of interest [15], or
- combinations of a dose gradient index with different indices for dose conformity, dose coverage, and dose homogeneity [16, 17].

The aforementioned dose gradient indices have an intrinsic shortcoming due to the one-dimensionality. The dose gradient indices described in [5-8, 10, 12, 13, 16, 17] were developed to irradiate small intracranial tumours and surgical cavities embedded in homogeneous brain tissue. However, all of the dose gradient indices provide only global information regarding the steepness of dose fall-off at the boundary of the target volume. As a result, dose gradient indices are not sufficient for evaluating the dose protection of multiple neighbouring organs at risk, for example, in the stereotactic radiotherapy for ocular tumours. For such cases, one must calculate the local dose gradients towards the organs at risk. Local information regarding the dose gradients is more expedient than one single global dose gradient value for the prediction of organ toxicities.

Consequently, the first definitions of more-dimensional dose gradient measures have been published in the years 2019 and 2021:

- The superficially averaged dose gradient *SADG* [18],
- the superficially averaged radius difference $\overline{\Delta r}_{\Delta D}$ [18], and
- the volumetrically averaged dose gradient *VADG* [19].

The utilisation of the aforementioned dose gradient measures is necessary to describe anisotropic dose gradient distributions at the boundary of the target volume due to the aforementioned shortcomings of the dose gradient indices. The aim must be to obtain meaningful quantifications of local dose gradients.

From a mathematical point of view, all of the dose gradient indices and measures can be divided into three categories:

I. Explicit [15, 18, 19],
II. inversely proportional or reciprocal [11, 13-15, 18], or
III. implicit [5-12, 16, 17].

These categories characterise the function type to describe the Euclidean norm $\|\nabla \cdot D(\boldsymbol{r})\| \in \mathbb{R}$ of the local physical dose gradient at an arbitrary position $\boldsymbol{r} \in \mathbb{R}^3$ or the global average of all of these dose gradient magnitudes by a certain dose gradient measure [18]. Based on the findings

in [11, 18, 19], it can be stated that explicit and reciprocal dose gradient measures better describe anisotropic dose gradient distributions than the implicit ones. Furthermore, the utilisation of implicit dose gradient measures may entail difficulties and inconsistencies in comparisons of dose gradients for different treatment techniques, irradiation modalities, patients, and irradiation series [11]. Consequently, the interpretation of clinical results regarding dose gradients by means of implicit dose gradient indices is extremely challenging.

All of the dose gradient measures are approximate specifications of clinical dose gradient distributions. The most precise description that can be numerically calculated will be the vector field of the dose gradients $\nabla \cdot D(\boldsymbol{r}) \in \mathbb{R}^3$ with the discretised dose matrix $D = D(\boldsymbol{r}) \in \mathbb{R}$ as a function of the position vector $\boldsymbol{r} \in \mathbb{R}^3$; the utilised treatment planning system yields this dose matrix. Consequently, the computational expense required for the calculation of values of the more-dimensional dose gradient measures is huge [18, 19]. Hereinafter, a real clinical dose gradient distribution is also called *physical dose gradients*.

On the other hand, the minimisation of computational expense with one-dimensional dose gradient indices possibly involves a considerable loss of accuracy whose degree is dependent on the anisotropy of the dose gradient distribution. Some dose gradient indices [12, 13, 16] assume isotropic dose gradient distributions despite the fact that even the isodoses of interest around globular brain lesions embedded in homogeneous tissue are not ideally ball-shaped [18]. By the way, all of the clinical dose gradient problems are anisotropic [19]. Anatomical and physical considerations do not permit centrally symmetric dose distributions in teletherapy of lesions in humans: Not one part of the human body is spherical, and not one spherical neoplasm or pathological protrusion will occur on the human body surface that could be irradiated from all of the directions within the entire solid angle $4 \cdot \pi$.

All of the gradient indices and measures aid in assessing treatment plans concerning clinical suitability and predicting the degree of severity of radiogenic side effects in critical structures. In this context, the quality of the description of a clinical dose gradient distribution is one necessary condition for the suitability of a dose gradient index or measure for predicting normal tissue complication probabilities. The existence of strong correlations between the values of a dose gradient measure and complication rates in the organs at risk is the highest maxim in the development of dose gradient measures to fulfil the aforementioned aim of ICRU Report no. 91. In this context, the clinical validity of correlations between the values of a dose gradient measure and treatment complications are not proved for all of the common dose gradient measures, with the exception of the volume of normal brain tissue, V_D, treated with at least the dose $D = 12\ Gy$ in one single-dose fraction.

Apart from dose conformity and dose gradients, another factor influences the clinical outcome in stereotactic radiotherapy. Nikova *et al.* revealed the connection between the kind of stereotactic radiosurgery apparatus and clinical outcomes in patients with brain metastases from primary lung cancer and renal carcinomas. They found links of the applied linear accelerator, CyberKnife® (Accuray, Inc., Sunnyvale, CA, USA), and Leksell Gamma Knife® (Elekta Instrument AB, Stockholm, Sweden) to local tumour control, local failure, and overall survival. For example, the values of Pearson's correlation coefficient for the correlations between local tumour control and type of apparatus were 0.354, 0.390, and 0.678 in case of the radiosurgery for metastases from lung cancer by linear accelerators, Gamma Knifes®, and CyberKnifes®, respectively [20]. The authors of this study quantified the dose fall-off at the target volume's boundary by means of the *GI* [5] that exhibits severe deficiencies as shown in [11]. The physical characterisation and rating of stereotactic radiosurgery machines and irradiation techniques concerning the producible dose gradients at the target volume's boundary could be stated more precisely through more-dimensional dose gradient measures.

The present article will assess the one-dimensional dose gradient indices that optimally quantify the mean value of the physical dose gradients. The two-dimensional *SADG* yielded reference values for this undertaking. All of the dose gradient measures were applied in one linac-based irradiation series for the stereotactic radiotherapy of 25 malignant

choroidal melanomas. Firstly, the values of the *SADG* were globally calculated for the nonspecific normal tissue. In addition, the values of the *SADG* were locally determined towards all of the organs at risk. The possible correlations between the global *SADG* and the other dose gradient measures were investigated. Furthermore, the correlations of all of the global dose gradient measures on the local *SADG* were analysed. Subsequently, possible correlations between the local *SADG* and dose-volume metrics that characterise the dose exposure of the organs at risk were examined. Besides, a novel geometrical measure called the relative ellipsoidality (E) was defined to quantify the degree of irregularity of target volumes and the degree of anisotropy of dose gradient problems.

2. MATERIALS AND METHODS

2.1. Definitions of common dose gradient indices

The anisotropic dose gradient measure *SADG* yield reference values to investigate the quality of all of the common dose gradient measures. For a better traceability of abbreviations in the text below, the common dose gradient measures are summarised with its abbreviations, mathematical categories, and referring references in Table A.1 of Appendix A.1.

The definitions of the volume ratio *VR* [8] and the quality index $f_{12\ Gy}$ [10] are listed there to draft a complete spread of the common dose gradient indices. In the following sections, they were no longer considered because the *VR* is a particular case of the dose gradient index *GI* [5], and the mathematical model for the calculation of $f_{12\ Gy}$ was not available.

2.2. Two-dimensional formulation of anisotropic dose gradient problems

The spatial distribution of the dose gradients at the boundary of the target volume is written in spherical coordinates because the dose gradients in the radial direction are of interest. For explanation, the radial dose gradient vectors are approximately perpendicular to the surfaces of the treated and irradiated volume and enable the description of the spatial dose gradient distributions. The system of spherical coordinates $K_S = \{O, r, \varphi, \vartheta\}$ is defined by the origin O in the geometrical mass centre of the planning target volume and the three curvilinear coordinates: radius r, azimuth φ, and polar distance angle ϑ.

From a mathematical perspective, the most simple anisotropic formulation is two-dimensional in φ and ϑ and will be linearised along r by the difference quotient. This is the rationale for the utilised dose gradient measure *SADG* as reference variable in this study. The exhaustive definition and explanation of the *SADG* is given in Appendix A.2 and [18].

2.2.1. Informative content of dose gradient distributions

The value of the *SADG* according to Eq. (A.1) is not the sole result because all of the local function values of the integrand

$$\frac{\Delta D}{\Delta r(\varphi,\vartheta)} = f(\varphi,\vartheta) \tag{1}$$

in Eq. (A.1), which quantify dose gradient distributions, are known during the integration process. Additionally, the values of further statistical measures of location and dispersion are available: median, modal value, range, standard deviation, and percentiles.

2.2.2. Algorithm for calculating the *SADG*

The algorithms for determining the *SADG* were implemented using MATLAB® R2007a (The MathWorks, Inc., Natick, MA, USA). The required geometrical and dosimetric input data for the solution of the two-dimensional dose gradient problem came from the utilised treatment planning system. The structure file `RS.*.dcm` and dose file `RD.*.dcm` in the DICOM data format were used to calculate the *SADG*. The pixel size was $p_x = p_y \equiv 0.78$ *mm* in computed axial tomography slices 1.00 *mm* thick. The unit cell of the dose grid had side lengths of $a = b \equiv 0.98$ *mm* and $c = 1.00$ *mm* in the DICOM coordinate directions x, y, and z, respectively.

2.3. Relative errors in the dose gradient indices

To quantify the deviations between a one-dimensional dose gradient index X and a more-dimensional dose gradient measure Z, the definition

$$\varepsilon(X)_Z = \frac{X - Z}{|Z|} \cdot 100\% \tag{2}$$

of the relative error was used. More generally, X is the value of an approximation, and Z is the value of the more exact quantity. The denominator in Eq. (2)

is the absolute value of Z and is called the reference value.

The superficially averaged radius difference according to Eq. (A.2) is the more exact reference value for calculating the relative errors in the dose gradient indices $\Delta R_{1/2}$, $DGI(D)$, and $\Delta r^{*}_{\Delta D}$; for explanations, see Table A.1.

The relative errors in the approximated $SADG^{*}|_{D_2}^{D_1}$ will be calculated with $Z = SADG(NT)|_{D_2}^{D_1}$. The more exact reference values of the errors in the $SADG_{RD}(NT)|_{D_2}^{D_1}$ are $Z_1 = SADG(NT)|_{D_2}^{D_1}$ according to Eq. (A.1) and $Z_2 = VADG_{proj}(NT)|_{D_2}^{D_1}$, where the three-dimensional $VADG_{proj}(NT)|_{D_2}^{D_1}$ is the most precise among all of the presented dose gradient measures. Its errors relative to Z_1 and Z_2 occur due to the discretisation of the isodoses of interest and linearization of the dose gradients in radial direction, respectively.

2.4. Quantity for characterising anisotropy of dose gradient problems

To quantitatively characterise the surface shapes of target volumes and isodoses of interest that can be approximately modelled by ellipsoids, the relative ellipsoidality (E) is defined as

$$\mathrm{E} = \frac{1}{b} \cdot \frac{(a-b)+(b-c)}{2} \geq 0\,, \tag{3}$$

where $a \geq b \geq c$ are the lengths of the semi-axes measured along three principal axes of a surface or volume. On that basis, E is a measure for the degree of anisotropy of dose gradient problems and for the degree of irregularity of target volumes. For example, the surface of a sphere with the radius R has the relative ellipsoidality E = 0 because $a = b = c \equiv R$; the property E = 0 is a synonym for ideal isotropy and regularity.

From a mathematical point of view, the ellipsoid is a second-order surface with the special cases $a = b$ (rotational ellipsoid) and $a = b =$ c (sphere). For a better understanding of the rationale for Eq. (3), the definition of the geometrical flattening of celestial bodies is given in Eq. (A.3) of Appendix A.4. The definition in Eq. (3) is a generalisation of the definition in Eq. (A.3) because the ellipsoid is a generalisation of the rotational ellipsoid.

2.5. Dosimetric and geometrical dependencies of organ doses

Figure 1 contains the schematic representation of the dose conditions at the boundary of a target volume and within organs at risk; it explains the dosimetric and geometrical dependencies of organ-specific dose levels. A distinction is made between two cases:

- The distance between the planning target volume (PTV) and an arbitrary organ at risk (OAR_i) varies at a constant dose gradient as shown in Figure 1a.
- The dose gradient at the planning target volume's boundary varies at a constant distance as shown in Figure 1b.

In both cases, the dose $D(OAR_i)$ within an arbitrary organ at risk OAR_i is a function of the dose gradient $dD_j / dr \approx \Delta D_j / \Delta r$ at the target volume's boundary and the distance r_i between both volumes of interest:

$$D(OAR_i) \approx D_{PI(PTV)} + \frac{\Delta D_j(r)}{\Delta r} \cdot r_i\,, \quad \frac{\Delta D_j(r)}{\Delta r} < 0\,. \tag{4}$$

The dose gradient was approximately described through the dose difference quotient $\Delta D_j / \Delta r$. $D_{PI(PTV)}$ is the dose level of the prescription isodose PI at the boundary of the planning target volume (PTV). The variable $D(OAR_i)$ is representative for various dose quantities: minimum dose D_{min}, maximum dose D_{max}, mean dose D_{mean}, median dose D_{median}, and other dose-volume metrics.

In practice, the two arguments $\Delta D_j / \Delta r$ and r_i of the function in Eq. (4) will not be systematically varied because the considered irradiation series is based on the anatomical conditions and clinical dose distributions. Besides, a systematic variation of local dose gradients would be extraordinarily challenging in consequence of the fact that local dose gradients are no optimisation parameters in the utilised treatment planning system.

Therefore, the author used the large variance of the irradiation series in both variables. The representation of the function $D(OAR_i) = f(\Delta D_j / \Delta r, r_i)$ can be accomplished in one single two-dimensional diagram: The values of the first argument will be applied along the abscissa; the varying distances between the ipsilateral organs at risk and the planning target volumes will be binned into discrete classes. Effectively, the diagram contains one graph per distance class.

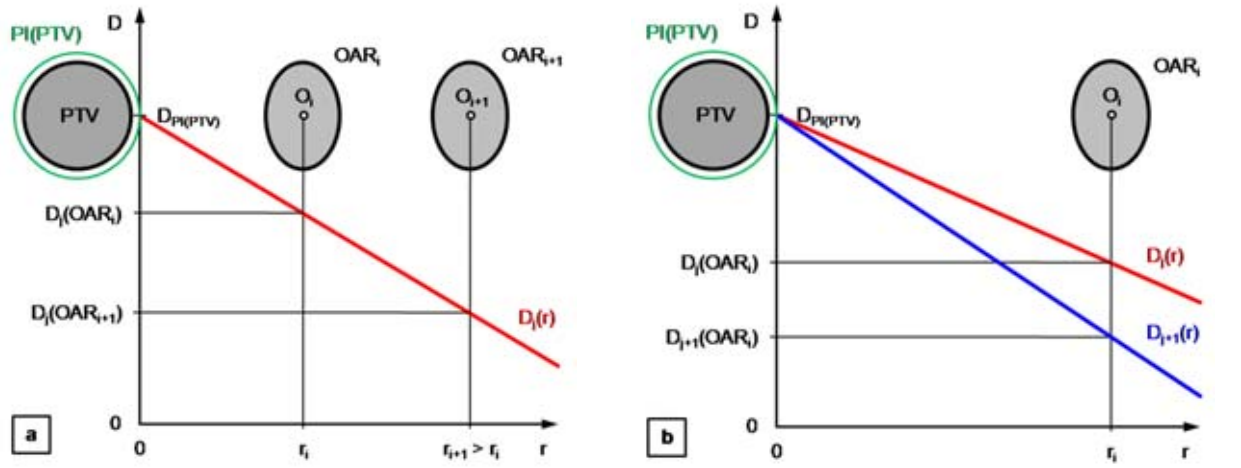

Figure 1. Schematic representation of dose conditions in organs at risk within the region of the dose fall-off at the boundary of a planning target volume: (a) variation of the distance between the planning target volume and the organ at risk at constant dose gradient and (b) variation of the dose gradient at constant distance. r - radius abscissa; D - dose ordinate; $PI(PTV)$ - prescribed isodose at the boundary of the planning target volume (PTV); $D_{PI(PTV)}$ - dose level of $PI(PTV)$; OAR_i, OAR_{i+1} - two arbitrary organs at risk; O_i, O_{i+1} - geometrical mass centres of the organs at risk; $D_j(r)$, $D_{j+1}(r)$ - two different linear courses of the dose fall-off at the target volume's boundary; r_i, r_{i+1} - distances between the prescribed isodose and the geometrical mass centres; $D_j(OAR_{i+1}) < D_j(OAR_i)$ - dose inequality for two different organs at risk with $r_{i+1} > r_i$ and at constant dose gradient $dD_j / dr = \Delta D_j/\Delta r$ = const.; $D_{j+1}(OAR_i) < D_j(OAR_i)$ - dose inequality for one organ at risk with $dD_{j+1} / dr < dD_j / dr$ and at constant distance r_i = const.

The organs at risk were divided into two types to select appropriate dose-volume metrics that characterize the dose exposure [2, 3]:

- The nonspecific normal tissue, eyeball, lacrimal gland, and lens oculi are structures with parallel anatomical architecture. Appropriate dose-volume metrics are the mean dose D_{mean} and the volume receiving at least the dose D, V_D.
- The cornea, optic nerve, and papilla are serially organised structures; the maximum dose D_{max} is an appropriate metric.

Depending on the type, the parameter that represents the second argument r_i of the function in Eq. (4) was chosen:

- For the parallel organs at risk, the superficially averaged distance $\overline{a}_{PTV-OAR_i}$ between the planning target volume and organ at risk was utilised.
- Through conclusion of analogy, the minimal distance a_{min} was used for the serial organs at risk. For a better understanding, the limit

$$\lim_{r_i \to a_{min}} \left[D_{PI(PTV)} + \frac{\Delta D_j(r)}{\Delta r} \cdot r_i \right] = D_{max}(OAR_i) \qquad (5)$$

of the function in Eq. (4) is equal to the maximum dose within the organ at risk.

The superficially averaged distance

$$\overline{a}_{PTV-OAR_i} = \frac{1}{\Omega_{OAR_i}} \cdot \int_{(\varphi_{OAR_i})} \int_{(\vartheta_{OAR_i})} \left[r_{OAR_i}(\varphi, \vartheta) - r_{PTV}(\varphi, \vartheta) \right] \cdot \sin\vartheta \cdot d\vartheta \cdot d\varphi \in \mathbb{R}^+ \qquad (6)$$

between the planning target volume (PTV) and an arbitrary organ at risk (OAR_i) will be defined in the coordinate system K_S explained in Subsection 2.2. The anisotropic radii $r_X(\varphi, \vartheta)$ with $X \in \{PTV, OAR_i\}$ are the lengths of the position vectors $r_X(\varphi, \vartheta) \in S(X)$ to the points of the surfaces $S(X)$ written in Cartesian coordinates of the system $K_C = \{O, x, y, z\}$, for example, DICOM coordinates.

The geometrical data of the surfaces are already present in Cartesian coordinates; for more information, see Subsection 2.2.2. Therefore, the following coordinate transformation given in [21] is necessary to perform the integration in Eq. (6):

$$\mathrm{K}_C \mapsto \mathrm{K}_S : \quad r = \sqrt{x^2 + y^2 + z^2}\,, \quad \varphi = \arctan\frac{y}{x}\,, \quad \vartheta = \arctan\frac{\sqrt{x^2 + y^2}}{z}. \tag{7}$$

The individual segment Ω_{OAR_i} of the entire solid angle is defined by the angle ranges φ_{OAR_i} and ϑ_{OAR_i}:

$$\left(\varphi_{OAR_i}, \vartheta_{OAR_i}\right) = \{(\varphi, \vartheta) \mid t \cdot \boldsymbol{r}(\varphi, \vartheta) \in S(OAR_i)\}\,, \quad \boldsymbol{r} = (x, y, z)^T\,, \quad t \in \mathbb{R}^+\,. \tag{8}$$

The multiplication factor t in Eq. (8) is a real positive number. Finally, the individual solid angle

$$\Omega_{OAR_i} = \int_{(\varphi_{OAR_i})} \int_{(\vartheta_{OAR_i})} dS \in \mathbb{R}^+\,, \quad dS \equiv d\Omega \tag{9}$$

follows from the application of the results of Eq. (8) to the definition of the solid angle, whereby dS and $d\Omega$ are the infinitesimal surface and solid angle elements. With the equivalence in Eq. (9), the surface integral in Eq. (6) can also be regarded as a solid angle integral. The minimal distance will be calculated with the integrand in Eq. (6):

$$a_{min} = \min_{\varphi \in (\varphi_{OAR_i}) \wedge \vartheta \in (\vartheta_{OAR_i})} \left[r_{OAR_i}(\varphi, \vartheta) - r_{PTV}(\varphi, \vartheta)\right]. \tag{10}$$

Based on Eq. (4), the author postulates dependencies of dose-volume metrics that characterise the dose distribution in an arbitrary organ at risk that is located in the region of the dose fall-off at the boundary of a target volume:

- The smaller the dose gradient or steeper the dose fall-off at the target volume's boundary, the lower the dose level in an organ at risk.
- The larger the distance from the target volume, the better the dose sparing in an organ at risk.

As a result, two complementary hypotheses will be formulated:

- Null hypothesis H_0: Dose-volume metrics that characterise the dose distributions in nonspecific normal tissue and organs at risk are independent of the dose fall-off at the target volume's boundary.
- Alternative hypothesis H_1: Tissue-specific dose-volume metrics strongly correlate on the dose gradients towards nonspecific normal tissue and organs at risk; the correlations are statistically significant.

2.6. Complication rates dependent on dose-volume metrics in organs at risk

One aim of the present article is to find possible correlations between treatment complication rates in organs at risk and the values of an appropriate dose gradient measure. The direct approach would be to conduct clinical studies with the objective of the assessment and classification of organ-specific radiogenic side effects; finally, the study results would be compared with the calculated values of a dose gradient measure.

To evade novel clinical studies that are laborious, another way in four steps will be followed:

1. Correlations between the utilised dose gradient measure and dose-volume metrics for the organs at risk can be analysed at low effort by the utilised treatment planning system and additional algorithms.
2. Already existing clinical study results that specify probabilities of radiogenic organ toxicities dependent on dose-volume metrics will be selected and exploited.
3. If a clinical study is based on irradiations with normal fractionation schemes and the present irradiation series is hypofractionatedly performed, the dose-volume metrics of the organs at risk will be corrected by a radiobiological model.
4. The composition of the results expressed under points 1 and 2 yields the wanted correlation for an arbitrary organ at risk – if there is one.

The aforementioned four-step approach shall be applied to the ipsilateral lacrimal glands. The author found an appropriate study that graded ocular

toxicities after the intensity-modulated radiotherapy for sinonasal tumours [22]. Details of the study are summarised in Appendix A.5 and Table A.2.

2.7. Linear-quadratic model of radiation biology

In accordance with step 3 of the specified approach in Subsection 2.6, tolerance dose values for the organs at risk have to be attuned to the utilised fractionation scheme. For this purpose, the linear-quadratic model of radiation biology [23] will be the basis to convert tolerance dose values between biologically equivalent fractionation schemes.

In accordance with the linear-quadratic model, the biologically effective dose (*BED*)

$$BED(TD) = TD_{norm} \cdot \left(1 + \frac{d_{norm}}{\alpha/\beta}\right) \equiv TD_{hypo} \cdot \left(1 + \frac{TD_{hypo}}{n_{hypo} \cdot \alpha/\beta}\right) \tag{11}$$

as a function of the tolerance dose TD for an arbitrary organ at risk is constant for equivalent fractionation schemes. TD_{norm} and d_{norm} are the tolerance dose and the dose per fraction of the normal fractionation, respectively. α/β is the tissue-dependent parameter of the cell survival curve. TD_{hypo} and n_{hypo} are the tolerance dose and the number of fractions of the hypofractionation, respectively.

The wanted tolerance dose

$$TD_{hypo} = \frac{n_{hypo} \cdot \alpha/\beta}{2} \cdot \left[-1 + \sqrt{1 + \frac{4 \cdot TD_{norm}}{n_{hypo} \cdot \alpha/\beta} \cdot \left(1 + \frac{d_{norm}}{\alpha/\beta}\right)}\right] \tag{12}$$

for the hypofractionation is one of the solutions of a quadratic equation that can be formed with the second and third terms of Eq. (11). The parameters to calculate the tolerance dose of an arbitrary organ at risk according to the conditions in the present irradiation series and in the utilised clinical study are: $n_{hypo} = 5$, $\alpha/\beta = 3$ *Gy* [23], $TD_{norm} = D_{mean}$, and $d_{norm} = 2$ *Gy*; D_{mean} is the mean dose for normal fractionation.

2.8. Statistics

Pearson's correlation coefficient r was used to quantify the strength of a correlation. The probability p of zero correlation was calculated using a one-sided association test based on Student's t test with $n - 2$ degrees of freedom, where n is the sample size. A significance level of $\alpha = 0.05$ was used; therefore, all confidence levels were $1 - \alpha = 0.95 \mathrel{\widehat{=}} 95\%$. The quality of estimating a correlation by a regression function was evaluated using the coefficient of determination r^2 [24].

2.9. Treatment and calculation parameters of irradiation series

The possible correlations of the examined dose gradient measures on the *SADG* were investigated using one irradiation series including 25 patients. The correlation analysis was performed for the clinically realised treatments of 25 malignant choroidal melanomas treated with the nominal tumour dose 50 *Gy* in five fractions.

15 dose gradient measures out of Table A.1 were determined for the linac-based stereotactic radiotherapy of 25 choroidal melanomas with a median planning target volume size of 1.84 cm^3 (range of 0.42 to 3.37 cm^3). The dose optimisation and calculation for the irradiation technique HybridArc™ were performed using the treatment planning system iPlan® RT Dose 4.5.3 and 4.5.4 (Brainlab AG, Munich, Germany); for details, see [15].

The irradiation machine was a Novalis powered by TrueBeam™ STx with a dynamic high-definition multi-leaf collimator HD 120™ (Brainlab AG, Munich, Germany and Varian Medical Systems, Inc., Palo Alto, CA, USA). The dose fractions were applied by 5.6 MV flattening filter-free photons with dose rates in a range of 800 to 1 400 *MU/min* (*MU* – monitor unit; normalised dose unit).

For comparability, the same isodoses of interest were used for the calculation of all of the dose gradient measures: The upper isodose level at the boundary of the planning target volume was always 86% and the lower isodose level was 43% of the prescribed tumour dose 50 *Gy*. The dose level 86% was the mean value of the minimum dose values within all of the planning target volumes and defined the treated volumes. Furthermore, the lower isodose at halved level is also used in the definitions of the common dose gradient indices.

The values of the *SADG* towards the nonspecific normal tissue and organs at risk were also calculated between the isodoses at the levels 95% and 20%. The dose level of 95% was the near-minimum dose according to ICRU Report no. 91 within all of the planning target volumes [3]. The lower dose level of 20% corresponds to 10 *Gy* in

five fractions that seems to be a harmless dose for all of the organs at risk. Additionally, the variation of the dose difference in the definition of the *SADG* enables an investigation of its influence on the values of the dose gradient measures.

3. RESULTS

3.1. Classification of dose gradient measures

Table A.1 summarises the characteristics of some classification features for all of the common dose gradient measures. They differ in unit, dimensionality, and type of mathematical description of a dose gradient distribution. The one-dimensionality and no explicit mathematical description of the physical dose gradients are common to all of the clinically utilised dose gradient indices; only the one-dimensional approximation $SADG^*$ of the *SADG* is an explicit dose gradient index. In contrast, the more-dimensional *SADG* and $VADG_{proj}$ are explicit dose gradient measures. The *SADG* and $VADG_{proj}$ exclusively enable anisotropic descriptions of real vector fields of the dose gradients.

3.2. Anisotropy of dose gradient problems

For the stereotactic radiotherapy of 25 malignant choroidal melanomas, Table 1 summarises the ranges, medians, mean values, and standard deviations of the volumes of interest, relative ellipsoidalities according to Eq. (3), and cardinalities of sets. These cardinalities are the sample sizes on which the calculations of the anisotropic dose gradient measures were based.

The relative ellipsoidalities of the isodoses of interest grew with a decreasing dose level: the range increased by 11.9% from 1/2.9 to 1/2.6 within the

Table 1. Sizes of the volumes of interest, relative ellipsoidalities, sample sizes, and relative errors in the approximated dose gradient measures for the stereotactic radiotherapy of 25 choroidal melanomas. V_{PTV} - size of the planning target volume; $V(D_1)$ - volume within the isodose at level $D_1 = 43.0$ *Gy* ≙ 86% relative to the nominal tumour dose 50 *Gy*; $V(D_2)$ - volume within the isodose at level $D_2 = 21.5$ *Gy* ≙ 43%; $E(X)$ - relative ellipsoidalities of $X \in \{V_{PTV},\ V(D_1),\ V(D_2)\}$ according to Eq. (3); $n(X)$ - sample sizes of $X \in \{SADG(NT)|_{D_2}^{D_1},\ SADG_{RD}(NT)|_{D_2}^{D_1},\ VADG_{proj}(NT)|_{D_2}^{D_1}\}$; $\varepsilon(X)_Z$ - relative errors with respect to the reference variables $Z \in \{SADG(NT)|_{D_2}^{D_1}, VADG_{proj}(NT)|_{D_2}^{D_1}\}$ in $X \in \{\Delta R_{1/2},\ DGI(D_2),\ \Delta r_{\Delta D}^*,\ SADG^*|_{D_2}^{D_1},\ SADG_{RD}(NT)|_{D_2}^{D_1}\}$ according to Eq. (2). For the formula symbols of the dose gradient measures, see Table A.1.

Quantity [Unit]	Minimum	Maximum	Median	Mean value	Standard deviation
V_{PTV} [cm^3]	0.42	3.37	1.84	1.83	0.98
$V(D_1)$ [cm^3]	0.50	4.73	2.41	2.52	1.39
$V(D_2)$ [cm^3]	2.84	15.54	9.07	8.88	3.95
E(V_{PTV}) [1]	1/13.8	1/2.5	1/5.5	1/5.4	1/13.9
E[$V(D_1)$] [1]	1/27.3	1/2.6	1/5.7	1/5.6	1/12.7
E[$V(D_2)$] [1]	1/11.5	1/2.1	1/5.9	1/5.4	1/12.0
$n[SADG(NT)|_{D_2}^{D_1}]$ [1]	1 194	5 248	2 848	2 772	1 128
$n[SADG_{RD}(NT)|_{D_2}^{D_1}]$ [1]	192	1 703	652	674	368
$n[VADG_{proj}(NT)|_{D_2}^{D_1}]$ [1]	2 182	17 488	6 854	7 103	3 769
$\varepsilon(\Delta R_{1/2})$ [%]	–3.2	18.4	2.4	5.1	6.2
$\varepsilon[DGI(D_2)]$ [%]	–11.8	8.6	–6.0	–4.3	6.5
$\varepsilon(\Delta r_{\Delta D}^*)$ [%]	–4.4	18.0	1.1	4.2	6.3
$\varepsilon(SADG^*|_{D_2}^{D_1})$ [%]	–4.6	15.3	1.1	3.7	5.6
$\varepsilon[SADG_{RD}(NT)|_{D_2}^{D_1}]_{SADG}$ [%]	–24.3	20.2	–9.2	–4.3	13.0
$\varepsilon[SADG_{RD}(NT)|_{D_2}^{D_1}]_{VADG}$ [%]	–18.8	–0.3	–8.4	–8.3	4.3

dose difference –21.5 *Gy* corresponding to –43% relating to the nominal tumour dose.

In another irradiation series for the stereotactic radiosurgery of 13 globular brain metastases defined in [11, 18, 19], the author found that the relative ellipsoidalities doubled between the isodose surfaces at the levels 80% and 40% relative to the particular maximum dose within the planning target volume, whereas the relative ellipsoidalities of the planning target volumes were exactly zero. The range, median, mean value, and standard deviation of E increased within the dose difference –40% from 1/32.4 to 1/16.1, 1/38.5 to 1/26.5, 1/38.8 to 1/21.4, and 1/113.1 to 1/45.5, respectively. The range of E doubled within the dose difference –40%.

3.3. Quality of dose gradient measures

15 dose gradient measures picked out of Table A.1 were determined for the stereotactic radiotherapy of 25 choroidal melanomas. The ranges, medians, mean values, and standard deviations of the errors in some dose gradient measures relative to the reference quantities *SADG* and $VADG_{proj}$ are listed in Table 1. The values of all of the dose gradient measures are shown in Figure 2.

The comparison of the errors in the one-dimensional dose gradient indices relative to the solution of the two-dimensional dose gradient problem according to Eq. (A.1) revealed the best range, median, mean value, and standard deviation of the relative errors in the approximated

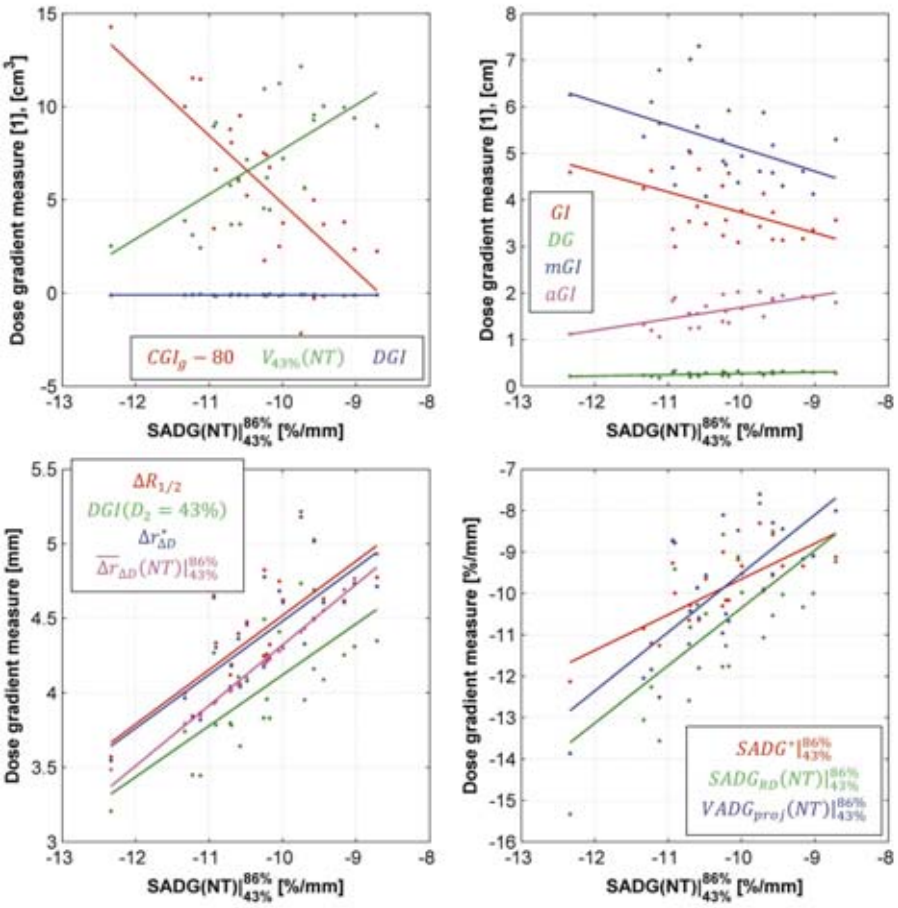

Figure 2. Correlations and regression lines $f(x) = m \cdot x + b$ of 14 different dose gradient measures on the reference variable $x = SADG(NT)|_{43\%}^{86\%}$ for the stereotactic radiotherapy of 25 malignant choroidal melanomas treated with the nominal tumour dose 50 *Gy* in five fractions. *m*, *b* - slope and ordinate intercept of a regression line; $SADG(NT)|_{43\%}^{86\%}$ - superficially averaged dose gradient for the nonspecific normal tissue (*NT*) according to Eq. (A.1); D_1 = 86%, D_2 = 43% - levels of the isodoses of interest relative to the nominal tumour dose; for the abbreviations of the 14 dependent dose gradient measures, see Table A.1 in Appendix A.1.

$SADG^*|_{43\%}^{86\%}$ defined in [15]: 19.9%, 1.1%, 3.7%, and 5.6%, respectively. The absolute values of the relative error were always ≤ 15.3% as given in Table 1.

The comparison of the values of the $SADG(NT)|_{D_2}^{D_1}$ given in Figure 2 and Table 2 lead to the statement that the dose gradient measure is dependent on the levels of the regarded isodoses of interest. The values were in a range of –12.3 to –8.7%/*mm* (median of –10.3%/*mm*) for the dose levels D_1 = 86% and D_2 = 43% relative to the nominal tumour dose 50 *Gy*. The dose gradient measure became values in a range of –8.4 to –5.4%/*mm* (median of –6.7%/*mm*) between the isodoses at the levels D_1 = 95% and D_2 = 20%.

The range, median, mean value, and standard deviation of the errors in the $SADG_{RD}$ relative to the *SADG* were 44.5%, –9.2%, and (–4.3 ± 13.0)%, whereas the reduction factor of the average sample size was 1/4.1 (see Table 1). The error range of 44.5% due to discretisation is more than twice the error range in the $SADG^*$ that is a result of one neglected dimension in the description of dose gradient problems.

Table 2. Sizes of the volumes of interest, dose-volume metrics, globally and locally defined superficially averaged dose gradients for nonspecific normal tissue and all of the ipsilaterally located organs at risk OAR_i, relative error in the approximated $SADG^*|_{D_2}^{D_1}$, sample sizes, as well as distances between the planning target volume and organs at risk for the stereotactic radiotherapy of 25 choroidal melanomas. *PTV*- planning target volume; *V* - sizes of the volumes of interest; *NT* - nonspecific normal tissue; $V(D_1)$ - volume within the isodose at level D_1= 47.5 *Gy* ≙ 95% relative to the nominal tumour dose 50 *Gy*; $V(D_2)$ - volume within the isodose at level D_2 = 10.0 *Gy* ≙ 20%; $V_{10\ Gy}$ - volume of normal tissue or of an organ at risk that receives at least the dose 10 *Gy*; $\varepsilon(V_{10\ Gy})$ - error in $V_{10\ Gy}$ relative to $V(D_2) - V(PTV)$ according to Eq. (2); $SADG^*|_{D_2}^{D_1}$ - spatially averaged dose gradient according to [15]; $SADG|_{D_2}^{D_1}$ - superficially averaged dose gradient for nonspecific normal tissue or towards an organ at risk according to Eq. (A.1); $\varepsilon(SADG^*|_{D_2}^{D_1})$ - error in $SADG^*|_{D_2}^{D_1}$ relative to $SADG(NT)|_{D_2}^{D_1}$ according to Eq. (2); *n* - sample size of the considered dose difference quotients to determine the *SADG*; D_{max} - maximum dose within an organ at risk; D_{mean} - mean dose value within an organ at risk; $\bar{a}$, a_{min} - superficially averaged and minimal distances between the planning target volume and organs at risk according to Eqs. (6) and (10).

Volume of interest	Quantity/dose gradient measure [Unit]	Minimum	Maximum	Median	Mean value	Standard deviation
PTV	$V\ [cm^3]$	0.42	3.37	1.84	1.83	0.98
Isodoses of interest	$V(D_1)\ [cm^3]$	0.17	3.17	1.49	1.54	0.96
	$V(D_2)\ [cm^3]$	9.21	50.59	29.33	27.13	12.15
	$V(D_2) - V(PTV)\ [cm^3]$	8.73	47.73	27.15	25.30	11.22
NT	$V_{10\ Gy}\ [cm^3]$[b]	9.30	53.60	30.10	27.78	12.51
	$\varepsilon(V_{10\ Gy})$ [%]	4.6	12.6	10.0	9.5	2.3
	$SADG^*|_{D_2}^{D_1}\ [\%/mm]$	–8.5	–5.3	–6.7	–6.7	0.8
	$SADG|_{D_2}^{D_1}\ [\%/mm]$	–8.4	–5.4	–6.7	–6.7	0.8
	$\varepsilon(SADG^*|_{D_2}^{D_1})\ [\%]$	–8.2	9.7	–1.3	–0.1	5.1
	n [1]	3 008	18 994	6 220	7 080	3 800
Cornea	$V\ [cm^3]$	0.05	0.22	0.17	0.16	0.04
	$D_{max}\ [Gy]$	0.8	44.9	3.8	9.0	11.1

Table 2 continued.

Cornea	$SADG\|_{D_2}^{D_1}$ [%/mm]	–15.0	–7.8	–10.9	–11.2	1.8
	a_{min} [mm]	0.5	15.8	11.0	9.7	4.6
	n [1]	176	514	358	353	91
Eye – PTV[a]	V [cm^3]	5.15	8.72	6.67	6.90	1.04
	D_{mean} [Gy]	8.4	26.6	14.6	15.8	4.8
	$SADG\|_{D_2}^{D_1}$ [%/mm]	–11.7	–6.2	–8.2	–8.3	1.3
	$\bar{a}$ [mm]	4.8	12.5	8.8	8.5	1.9
	n [1]	1 836	3 370	2 510	2 549	324
Lacrimal gland	V [cm^3]	0.23	1.44	0.50	0.54	0.27
	$V_{10\ Gy}$ [%]	0.0	100.0	25.6	40.4	39.7
	D_{mean} [Gy]	1.0	21.4	8.2	10.2	6.5
	$SADG\|_{D_2}^{D_1}$ [%/mm]	–14.2	–4.8	–7.6	–8.1	2.1
	$\bar{a}$ [mm]	2.8	17.0	9.7	10.6	3.8
	n [1]	256	1 114	434	487	204
Lens oculi	V [cm^3]	0.13	0.34	0.26	0.25	0.05
	D_{mean} [Gy]	0.7	48.1	1.9	5.6	10.2
	$SADG\|_{D_2}^{D_1}$ [%/mm]	–15.2	–8.2	–10.6	–11.0	1.9
	$\bar{a}$ [mm]	2.2	15.3	11.5	9.8	3.8
	n [1]	146	366	238	235	50
Optic nerve	V [cm^3]	0.33	0.83	0.56	0.57	0.12
	D_{max} [Gy]	8.4	51.8	50.4	45.0	10.8
	$SADG\|_{D_2}^{D_1}$ [%/mm]	–13.9	–4.2	–10.0	–9.5	2.3
	a_{min} [mm]	0.0	9.3	0.0	0.7	1.9
	n [1]	416	992	636	631	133
Papilla	V [cm^3]	0.01	0.06	0.03	0.03	0.01
	D_{max} [Gy]	8.4	51.8	50.4	45.0	10.8
	$SADG\|_{D_2}^{D_1}$ [%/mm]	–12.6	–4.4	–9.0	–9.1	2.0
	a_{min} [mm]	0.0	8.4	0.0	0.5	1.7
	n [1]	34	172	92	94	36

[a]Healthy sections of the eyeball include the ciliary body, macula lutea, and retina. [b]Results out of dose-volume histograms.

Otherwise, the range, median, mean value, and standard deviation of the errors in the $SADG_{RD}$ relative to the $VADG_{proj}$ were 18.5%, –8.4%, and (–8.3 ± 4.3)%, whereas the reduction factor of the average sample size was 1/10.5 (see Table 1). The error range of 18.5% due to linearisation is nearly equal to the error range in the $SADG^*$.

3.4. Correlation analyses between globally defined dose gradient measures

The $SADG(NT)|_{D_2}^{D_1}$ was picked out of a set of 15 different dose gradient measures to be the reference variable for the correlation analyses between the dose gradient measures for the stereotactic radiotherapy of 25 choroidal melanomas. The correlations and regression lines of 14 dose gradient measures are summarised in Figure 2. The analyses' objective is to grade the dose gradient measures by the strengths of correlation on the mean value of the physical dose gradients described by a more-dimensional measure. The corresponding absolute values of Pearson's correlation coefficient r are presented in Figure 3. The probabilities of zero correlation were in a range of $p \in [7.0 \cdot 10^{-24}, 1.0 \cdot 10^{-2}]$, with exception of the *DGI* ($p = 5.6 \cdot 10^{-1}$).

The superficially averaged radius difference $\overline{\Delta r}_{\Delta D}(NT)|_{D_2}^{D_1}$ showed the strongest correlation with $r = 0.994$ in the group of the more-dimensional dose gradient measures. Pearson's correlation coefficients r of the two-dimensional $SADG_{RD}(NT)|_{D_2}^{D_1}$ and the three-dimensional $VADG_{proj}(NT)|_{D_2}^{D_1}$ were 0.646 and 0.744, respectively. In the group of the one-dimensional dose gradient indices, the $SADG^*|_{D_2}^{D_1}$ was second to none because $r = 0.785$ was best. The inversely proportional dose gradient indices exhibited stronger correlations with $r \in [0.661, 0.770]$ than the implicit dose gradient indices, with exception of the CGI_g ($r = -0.770$). Pearson's correlation coefficients of any other implicit dose gradient indices were in a range of $|r| \in [0.124, 0.660]$.

The trends in 14 dose gradient measures on an increasing reference variable were also examined. The dose gradient indices *GI*, *DG*, *mGI*, and *DGI* showed false positive trends on an increasing value of the $SADG(NT)|_{D_2}^{D_1}$ in Figure 2. Although Figure 2 shows a constant regression line for the *DGI* because of the large scale of the ordinate, $r = -0.124$ indicates the false positive trend.

3.5. Globally and locally defined dose gradient measures

The *SADG* towards the nonspecific normal tissue and the ipsilaterally located organs at risk were determined between the isodoses of interest at the levels $D_1 = 95\%$ and $D_2 = 20\%$ relative to the prescribed tumour dose 50 *Gy* for the stereotactic radiotherapy of the 25 choroidal melanomas. The organs at risk are the cornea, healthy sections of the eyeball – including the ciliary body, macula lutea, as well as retina –, lacrimal gland, lens oculi, optic nerve, and papilla. Table 2 summarises the ranges, medians, mean values, and standard deviations of the volumes of interest, global and local dose gradient measures, dose-volume metrics, distances according to Eqs. (6) and (10), as well as sample sizes.

The values of the dose-volume metric $V_{10\ Gy}(NT)$ that will be needed for correlation analyses on the globally defined *SADG* differed from the values of the equivalent difference volumes $V(D_2) - V(PTV)$ given in Table 2. The data sources in the utilised treatment planning system were different: The values of $V_{10\ Gy}$ were extracted out of the cumulative dose-volume histograms for the nonspecific normal tissue; the equivalent difference volumes were calculated with the volumes that are encompassed by the isodoses of interest at the level $D_2 = 10$ *Gy* as well as the sizes of the planning target volumes. The errors in the values of $V_{10\ Gy}(NT)$ relative to the equivalent difference volume were in a range of 4.6 to 12.6% (median of 10.0%).

According to the absolute value, the error in the $SADG^*$ relative to the two-dimensional *SADG* was always $\leq 9.7\%$ for the nonspecific normal tissue. The minimum values of the locally defined *SADG* towards the organs at risk were in a range of –15.2 to –11.7%/*mm*; the range of the corresponding mean values was –11.2 to –8.1%/*mm*. In contrast, the minimum and mean values of the globally defined *SADG* towards the nonspecific normal tissue were –8.4%/*mm* and –6.7%/*mm*, respectively. Figure 4 represents the values of the globally and locally defined *SADG* for all of the 25 patients. For example, the mean values of the locally defined *SADG* were 1.2 to 1.7 times smaller than the mean value of the globally defined *SADG*. In other words, the local dose gradients were always distinctly steeper than the corresponding global dose gradients.

The values of the *SADG* for the nonspecific normal tissue were in a range of –8.4 to –5.4%/*mm* with a median of –6.7%/*mm* according to Table 2. The corresponding values with the isodoses of interest

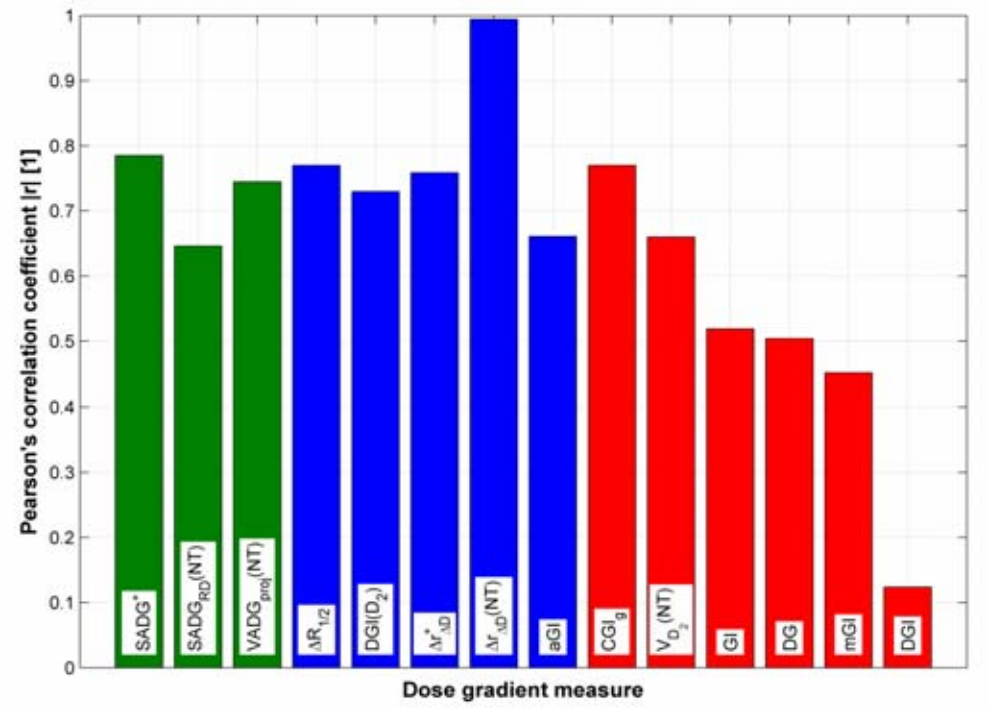

Figure 3

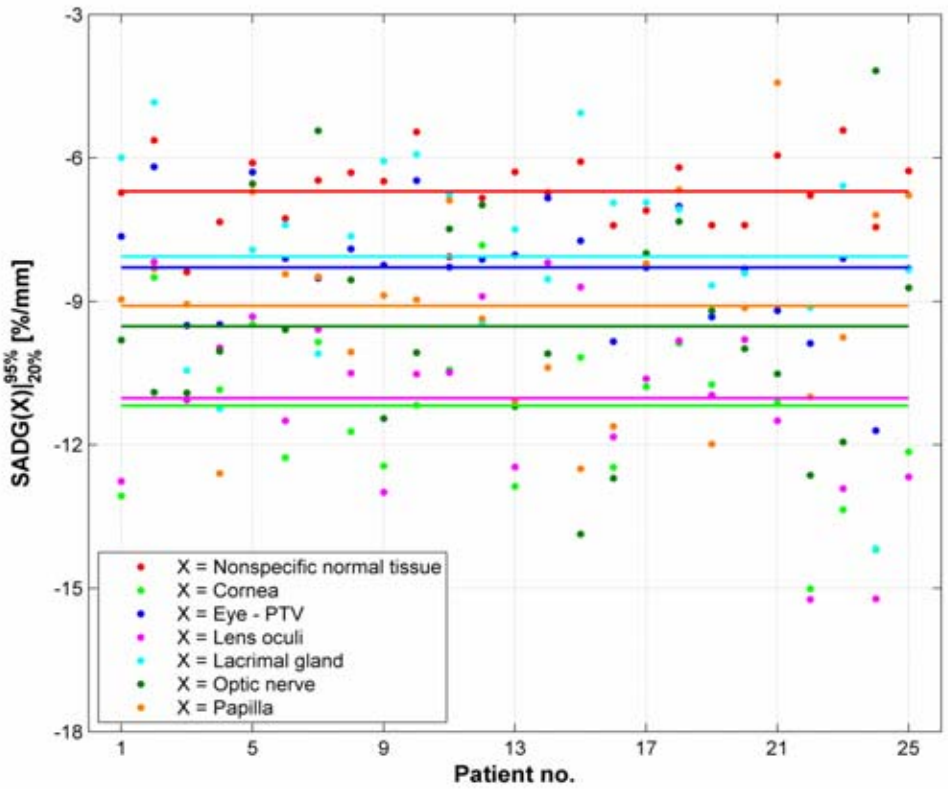

Figure 4

at the levels 86% and 43% were in a range of –12.3 to –8.7%/*mm* (median of –10.3%/*mm*); for details, see Figure 2.

3.6. Correlation analyses between globally and locally defined dose gradient measures

One of the findings noted in Subsection 3.2 was that the dose gradient problems in the examined irradiation series exhibit a high degree of anisotropy. This circumstance raises the question concerning the description quality of such dose gradient problems by globally defined dose gradient measures. In response to this fundamental question, correlation analyses of globally defined dose gradient measures on the locally defined *SADG* towards one organ at risk – the ipsilateral lacrimal gland – were performed.

The absolute values of Pearson's correlation coefficient are summarised in Figure 5. All of the correlations were weak with $|r| \in [0.034, 0.404]$ and $p \in [4.5 \cdot 10^{-2}, 8.7 \cdot 10^{-1}]$. The best results showed the two-dimensional dose gradient measures $\overline{\Delta r}_{\Delta D}(NT)|_{D_2}^{D_1}$ and $SADG(NT)|_{D_2}^{D_1}$ with $r = 0.404$ ($p = 4.5 \cdot 10^{-2}$) and $r = 0.397$ ($p = 5.0 \cdot 10^{-2}$), respectively. The correlations of any other dose gradient measures were statistically not significant.

3.7. Correlation analyses between dose gradients and dose-volume metrics

The dependencies of dose-volume metrics for organs at risk on dosimetric and geometrical parameters in the region of the dose fall-off at the boundary of a target volume were deduced and explained in Subsection 2.5. Correlations of dose-volume metrics for the nonspecific normal tissue and the ipsilateral organs at risk on the locally defined dose gradient measure at the target volume's boundary were analysed.

The results are represented by diagrams specified in Subsection 2.5 for the considered irradiation series involving 25 malignant choroidal melanoma cases. The correlation analyses for the ipsilateral lacrimal glands were performed for two classes of the superficially averaged distance between the planning target volume (*PTV*) and the organ at risk (OAR_i): $\overline{a}_{PTV-OAR_i} \in]5, 10]\ mm$ and $\overline{a}_{PTV-OAR_i} \in]10, 15]\ mm$.

The correlation of $V_{10\ Gy}\ (NT)$ for the nonspecific normal tissue on the globally defined $SADG(NT)|_{20\%}^{95\%}$ was strong and statistically significant, whereby Pearson's correlation coefficient and the probability of zero correlation were $r = 0.833$ and $p = 2.4 \cdot 10^{-7}$, respectively. The associated regression line obeyed the function $f(x) = 13.547\ cm^3 \cdot mm \cdot \%^{-1} \cdot x + 118.567\ cm^3$. Figure 6 shows the correlation and regression line.

For the ipsilateral lacrimal glands, the correlation of $V_{10\ Gy}(OAR_i)$ on the locally defined $SADG(OAR_i)|_{20\%}^{95\%}$ was strong and statistically significant in the first distance class, whereby $r = 0.879$ ($p = 4.0 \cdot 10^{-3}$). The associated regression line obeyed the function $f(x) = 15.289\ mm \cdot x + 183.408\%$. The correlation

Legend to Figure 3. Absolute values of Pearson's correlation coefficient *r* that rate the 14 dependent dose gradient measures for the nonspecific normal tissue (NT) on the reference variable $SADG(NT)|_{43\%}^{86\%}$ with regard to the strength of correlation. The green, blue, and red bars represent explicit, reciprocal, and implicit dose gradient measures, respectively. $SADG(NT)|_{43\%}^{86\%}$ - superficially averaged dose gradient for the nonspecific normal tissue according to Eq. (A.1); $D_1 = 86\%$, $D_2 = 43\%$ - levels of the isodoses of interest relative to the nominal tumour dose 50 *Gy*; for the abbreviations of the 14 dependent dose gradient measures, see Table A.1 in Appendix A.1.

Legend to Figure 4. Global and local values of the superficially averaged dose gradient $SADG(X)|_{20\%}^{95\%}$ for the stereotactic radiotherapy of 25 choroidal melanomas in 25 different patients. The horizontal lines depict the particular mean values calculated from all of the 25 patients. *X* - tissue type of the ipsilateral eye; *PTV* - planning target volume; *Eye–PTV* - difference volume between the whole eyeball and the planning target volume; $D_1 = 95\%$, $D_2 = 20\%$ - levels of the proximal and distal isodoses of interest, respectively, relative to the nominal tumour dose 50 *Gy*; for the definition of the $SADG(X)|_{20\%}^{95\%}$, see Appendix A.2.

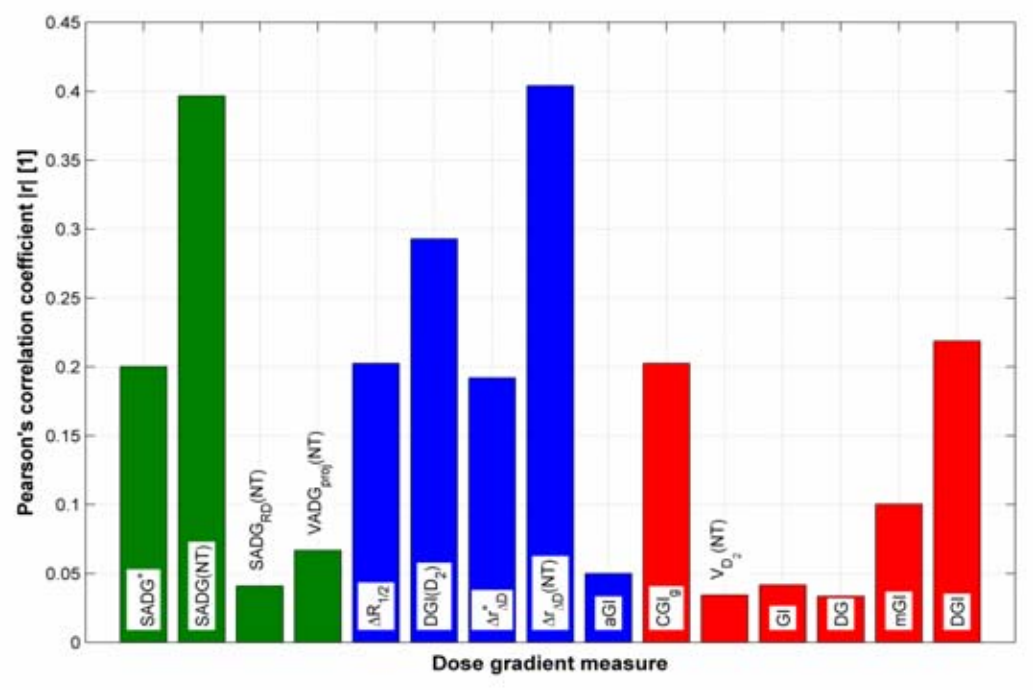

Figure 5

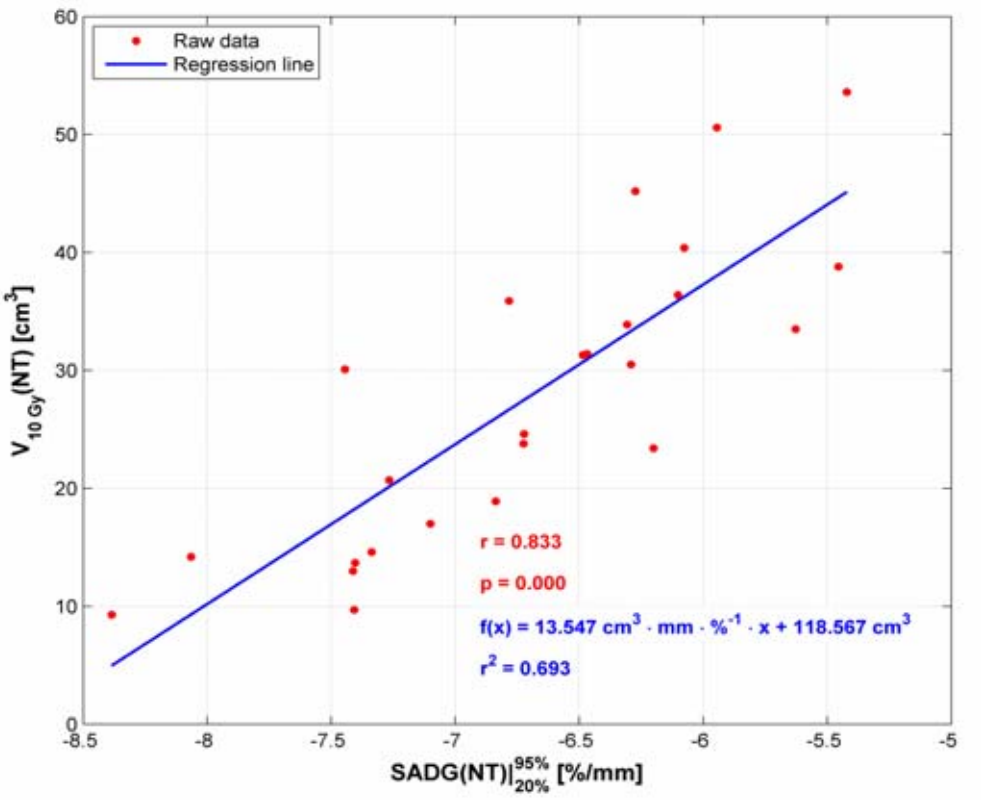

Figure 6

in the second distance class was also strong and statistically significant, whereby r = 0.899 (p = $6.0 \cdot 10^{-3}$). The corresponding regression function was $f(x)$ = 6.882 $mm \cdot x$ + 67.186%. Figure 7 shows the correlations and regression lines.

The correlation of $D_{mean}(OAR_i)$ for the ipsilateral lacrimal glands on the locally defined $SADG(OAR_i)|_{20\%}^{95\%}$ was strong and statistically significant in the first distance class, whereby r = 0.870 (p = $4.9 \cdot 10^{-4}$). The associated regression line obeyed the function $f(x)$ = 2.580 $Gy \cdot \%^{-1} \cdot mm \cdot x$ + 33.665 Gy. The correlation in the second distance class was also strong and statistically significant, whereby r = 0.957 (p = $5.2 \cdot 10^{-5}$). The corresponding regression function was $f(x)$ = 1.565 $Gy \cdot \%^{-1} \cdot mm \cdot x$ + 17.901 Gy. Figure 8 shows the correlations and regression lines.

Table 3 summarises the results of the correlation analyses for all further ipsilateral organs at risk: cornea, eyeball, lens oculi, optic nerve, and papilla.

Table 3. Correlations of characteristic dose metrics in the ipsilateral organs at risk on the locally defined $SADG(OAR_i)|_{D_2}^{D_1}$ for the stereotactic radiotherapy of 25 choroidal melanomas; D_1 = 95% relative to the nominal tumour dose 50 Gy, D_2 = 20%. a_1, a_2 - lower and upper interval boundaries of the distance between the planning target volume and organ at risk; r - Pearson's correlation coefficient; p - probability of zero correlation; m, b - slope and ordinate intercept of the regression line.

Organ at risk	Type[a]	a_1 [mm]	a_2 [mm]	r [1]	p [1]	m [$Gy \cdot \%^{-1} \cdot mm$]	b [Gy]
Cornea	Serial	7.50	12.50	0.744	$3.4 \cdot 10^{-2}$	1.683	22.436
		12.50	17.50	0.836	$5.0 \cdot 10^{-3}$	0.885	11.023
Eye – PTV[b]	Parallel	2.50	7.50	0.737	$3.7 \cdot 10^{-2}$	2.780	42.876
		7.50	12.50	0.802	$1.1 \cdot 10^{-4}$	2.777	36.971
Lens oculi	Parallel	2.50	7.50	0.843	$1.7 \cdot 10^{-2}$	3.127	48.852
		7.50	12.50	0.646	$3.2 \cdot 10^{-2}$	0.893	11.740
Optic nerve	Serial	0.00	0.75	0.581	$7.2 \cdot 10^{-3}$	1.553	62.376
Papilla	Serial	0.00	0.75	0.461	$3.6 \cdot 10^{-2}$	1.564	62.339

[a]Specification of the anatomical architecture of the organ at risk [2, 3]. [b]Healthy sections of the eyeball include the ciliary body, macula lutea, and retina.

Legend to Figure 5. Absolute values of Pearson's correlation coefficient r that rate 15 globally defined dose gradient measures for the nonspecific normal tissue (NT) on the locally defined reference variable $SADG(OAR_i)|_{20\%}^{95\%}$ with regard to the strength of correlation. The green, blue, and red bars represent explicit, reciprocal, and implicit dose gradient measures, respectively. $SADG(OAR_i)|_{20\%}^{95\%}$ - superficially averaged dose gradient for the ipsilateral lacrimal gland (organ at risk OAR_i) according to Eq. (A.1); D_1 = 95%, D_2 = 20% - dose levels of the isodoses of interest relative to the nominal tumour dose 50 Gy; for the abbreviations of the 15 dependent dose gradient measures, see Table A.1 in Appendix A.1.

Legend to Figure 6. Correlation and regression line of the dose-volume metric $V_{10\ Gy}(NT)$ on the dose gradient measure $x = SADG(NT)|_{20\%}^{95\%}$ for the stereotactic radiotherapy of 25 choroidal melanomas. $SADG(NT)|_{20\%}^{95\%}$ - superficially averaged dose gradient for the nonspecific normal tissue (NT) according to Eq. (A.1); $V_{10\ Gy}(NT)$ - volume of the nonspecific normal tissue that receives at least 10 Gy; r - Pearson's correlation coefficient; p - probability of zero correlation; $f(x)$ - linear equation of the regression line; r^2 - coefficient of determination.

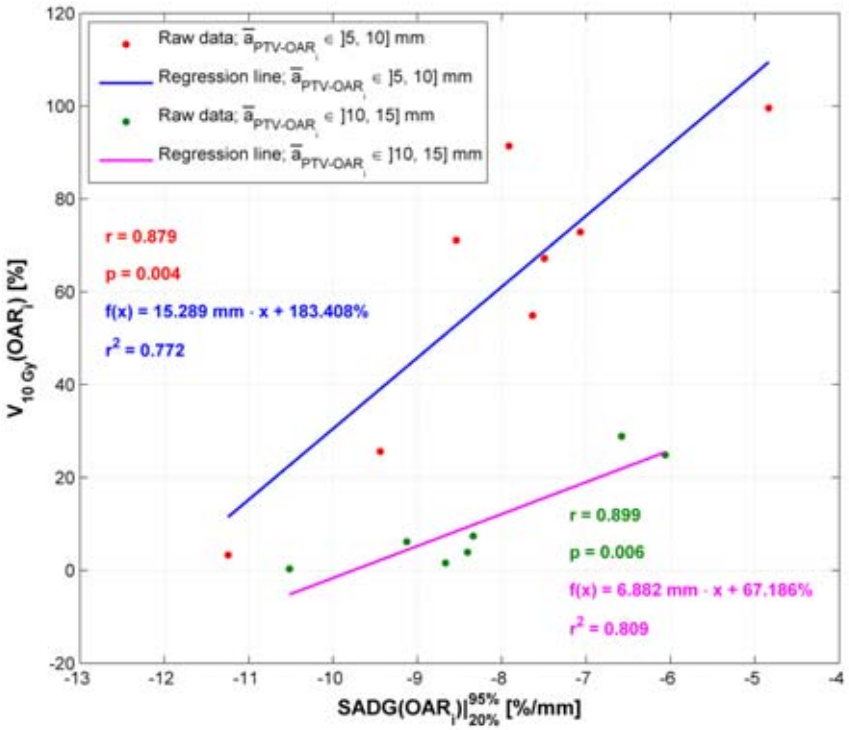

Figure 7

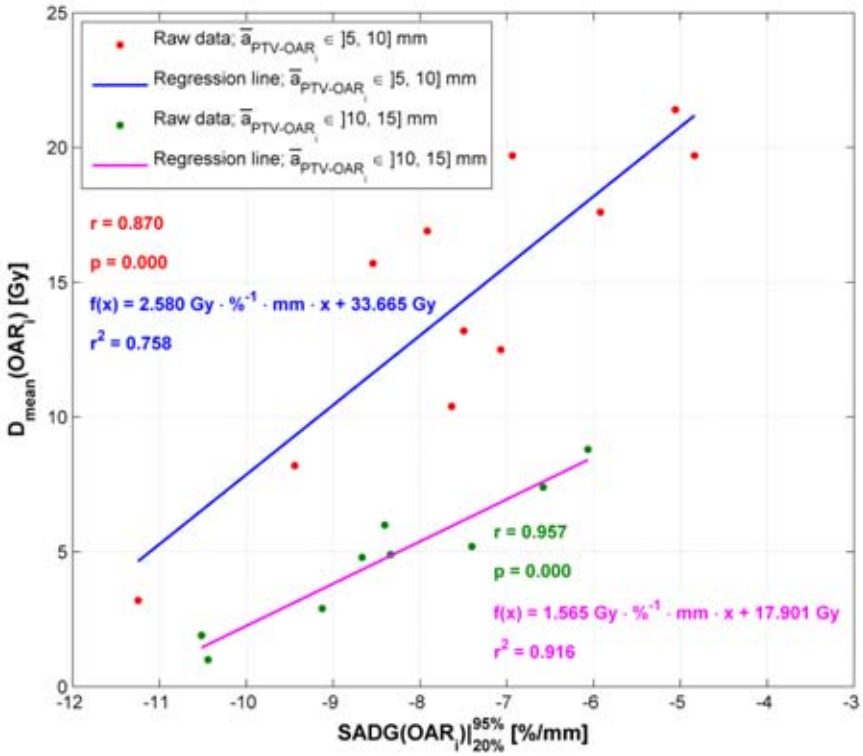

Figure 8

The intervals for the distances between the planning target volumes and organs at risk should be understood as $a_{min} \in]a_1, a_2]$ and $\overline{a}_{PTV-OAR_i} \in]a_1, a_2]$ for the serial and parallel organs at risk, respectively. The values of r and p indicated strong correlations that were statistically significant. The associated regression lines obeyed the function $f(x) = m \cdot x + b$ with $x = SADG(OAR_i)|_{20\%}^{95\%}$.

Based on the results of the performed correlation analyses, the alternative hypothesis was accepted for the nonspecific normal tissue and all of the organs at risk; consequently, the related null hypothesis was rejected. For the formulations of the hypotheses, see the last paragraph of Subsection 2.5.

3.8. Correlations between local dose gradients and complication rates

Through the results in Subsection 3.7 and Figure 8, the mean dose values in Table A.2 can be replaced by the correlating values of the locally defined

Table 4. Incidences of acute and late ocular toxicities of grade 2 or higher dependent on the local dose gradient towards the ipsilateral lacrimal gland that can occur after the stereotactic radiotherapy for malignant choroidal melanomas; grading according to the radiation toxicity criteria of [25]. $SADG(OAR_i)|_{D_2}^{D_1}$ - locally defined superficially averaged dose gradient; OAR_i - organ at risk that is here the ipsilateral lacrimal gland; D_1 - level of the proximal isodose of interest that has here the level 95% relative to the nominal tumour dose 50 *Gy*; D_2 - level of the distal isodose of interest that has here the level 20%; $\overline{a}_{PTV-OAR_i}$ - superficially averaged distance between the planning target volume (*PTV*) and the organ at risk (OAR_i) according to Eq. (6).

$SADG(OAR_i)\|_{D_2}^{D_1}$ [%/mm]		Incidence of acute toxicity [%]	Incidence of late toxicity [%]
$\overline{a}_{PTV-OAR_i} \in]5, 10]\ mm$	$\overline{a}_{PTV-OAR_i} \in]10, 15]\ mm$		
∈[–12.5, –10.7[	∈[–10.5, –7.6[	0.0	0.0
∈[–10.7, –7.9[	∈[–7.6, –3.0[	12.5	12.5
∈[–7.9, –5.8[	∈[–3.0, 0.4[[a]	57.1	28.6
∈[–5.8, –4.1[	∈[0.4, 3.3[[a]	80.0	60.0
≥ –4.1	≥ 3.3[a]	100.0	100.0

[a]The positive dose gradient values are purely hypothetical and results of the underlying regression line shown in Figure 8.

Legend to Figure 7. Correlations and regression lines of the dose-volume metric $V_{10\ Gy}(OAR_i)$ on the dose gradient measure $x = SADG(OAR_i)|_{20\%}^{95\%}$ for the stereotactic radiotherapy of 15 choroidal melanomas. $SADG(OAR_i)|_{20\%}^{95\%}$ - superficially averaged dose gradient towards the ipsilateral lacrimal glands (organs at risk OAR_i) according to Eq. (A.1); $V_{10\ Gy}(OAR_i)$ - volume of the organ at risk that receives at least 10 *Gy*; $\overline{a}_{PTV-OAR_i}$ - superficially averaged distance between the target volume (*PTV*) and the organ at risk according to Eq. (6); r - Pearson's correlation coefficient; p - probability of zero correlation; $f(x)$ - linear equation of a regression line; r^2 - coefficient of determination.

Legend to Figure 8. Correlations and regression lines of the mean dose $D_{mean}(OAR_i)$ on the dose gradient measure $x = SADG(OAR_i)|_{20\%}^{95\%}$ for the stereotactic radiotherapy of 20 choroidal melanomas. $SADG(OAR_i)|_{20\%}^{95\%}$ - superficially averaged dose gradient towards the ipsilateral lacrimal glands (organs at risk OAR_i) according to Eq. (A.1); $D_{mean}(OAR_i)$ - mean dose within the organ at risk; $\overline{a}_{PTV-OAR_i}$ - superficially averaged distance between the target volume (*PTV*) and the organ at risk according to Eq. (6); r - Pearson's correlation coefficient; p - probability of zero correlation; $f(x)$ - linear equation of a regression line; r^2 - coefficient of determination.

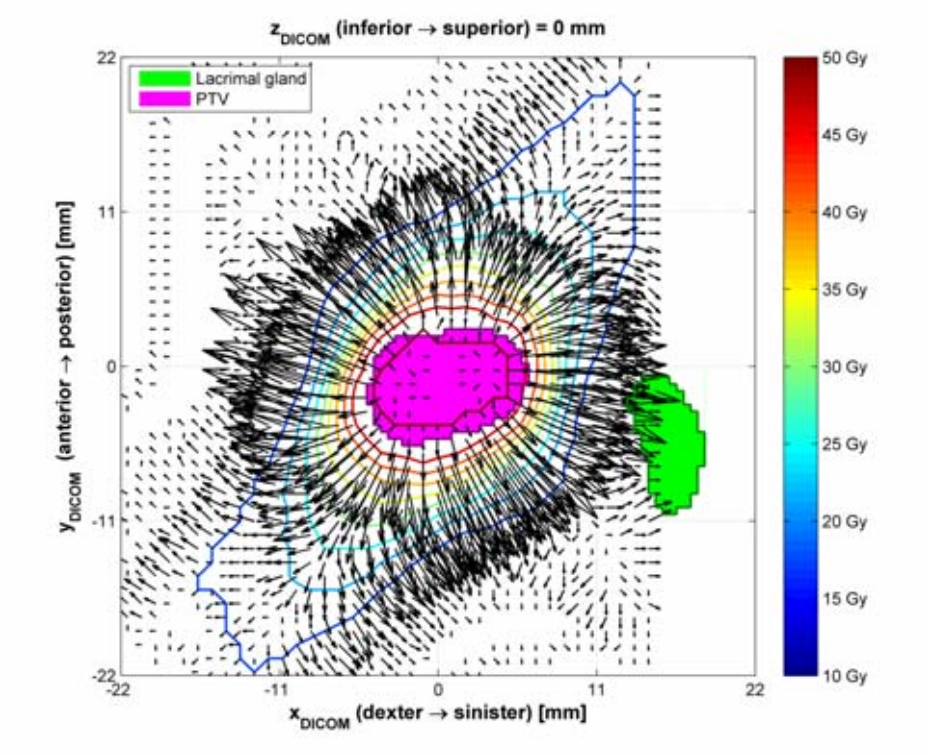

Figure 9

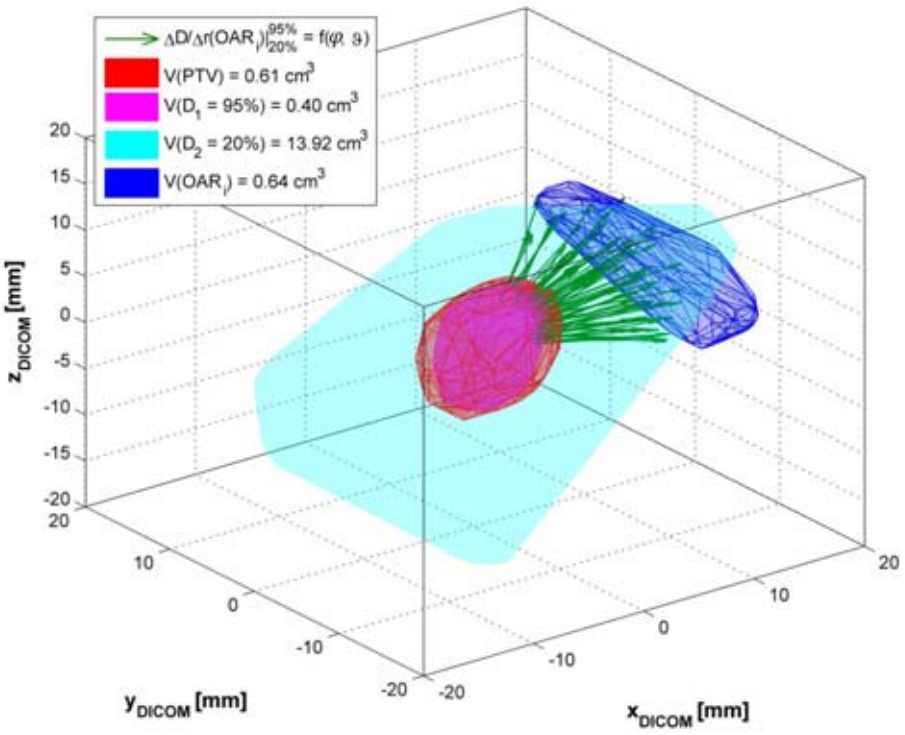

Figure 10

dose gradient measure $SADG(OAR_i)|_{D_2}^{D_1}$. In doing so, the tolerable mean dose values of a lacrimal gland have to be converted according to Eq. (12) because Table A.2 is based on the normal fractionation and the present irradiation series was performed with hypofractionation.

The fourth column of Table A.2 contains the converted tolerance dose values for the hypofractionation. The final outcome is the content of Table 4 that yields incidences of acute and late ocular toxicities of grade 2 or higher as functions of the locally defined dose gradient measure and the superficially averaged distance between the planning target volume and the ipsilateral lacrimal gland. The smaller the value of the $SADG(OAR_i)|_{D_2}^{D_1}$ and the greater the value of $\overline{a}_{PTV-OAR_i}$, the lower the risk to the incidence of acute and late toxicities.

3.9. Graphical representations of anisotropic dose gradient distributions

Visualisations of the dose gradients will be presented for one of the 25 choroidal melanoma cases. The laterally located tumour directly next to the papilla and in the caudal hemisphere of the left eyeball had a volume of 0.10 cm^3, and the size of the treated planning target volume was 0.61 cm^3. The volume of the ipsilateral lacrimal gland was 0.64 cm^3 in patient no. 4.

Figure 9 represents the anisotropic distribution of the dose gradients as a vector field in the isocentric axial plane with isodose lines in 5 *Gy* steps within a range of 10 to 50 *Gy*. The black arrows symbolise the dose gradient vectors $\nabla \cdot D(x, y, z = 0\ mm)$ in a Cartesian coordinate system specified by the anatomical directions given in Figure 9 and point in the direction of decreasing dose. The distances between all of the pairs of isodose lines and the vector lengths are obviously functions on the circumferential angle. This circumstance verifies the strong anisotropy of the present dose gradient distribution. The relative ellipsoidalities of the isodoses of interest at the levels 86% and 43% exhibited high values: 1/5.0 and 1/6.9, respectively.

The short vector lengths within the isodose line at the level 45 *Gy* in Figure 9 indicated good dose homogeneity within the planning target volume.

Figure 10 shows the planning target volume, isodoses of interest at the levels 95% and 20% relative to the nominal tumour dose 50 *Gy*, and ipsilateral lacrimal gland in three dimensions for the same patient. The green vector bundle represents the local dose difference quotients $\Delta D/\Delta r(\varphi, \vartheta)$ towards the lacrimal gland in the direction of the dose fall-off. The dose difference is ΔD = 75% = const.; $\Delta r\ (\varphi, \vartheta)$ is the distance between the isodoses of interest as a function of the azimuth φ and polar distance angle ϑ.

4. DISCUSSION

4.1. Anisotropy of dose gradient problems

The small values of the relative ellipsoidality E for the stereotactic radiosurgery of 13 globular brain metastases defined in [11, 18, 19] compared

Legend to Figure 9. Isocentric axial section through the vector field of the dose gradients with isodose lines for the stereotactic radiotherapy of the choroidal melanoma in patient no. 4 specified in Subsection 3.9. The black arrows are the dose gradient vectors in a discrete dose grid with a lattice parameter of 0.98 *mm*; the scale is 7.5 *mm*/(1 *Gy*/*mm*). The magenta area represents the cross sectional area of the planning target volume (*PTV*); the grass-green area is the cross sectional area of the ipsilateral lacrimal gland; nine different isodose lines at the levels (10 : 5 : 50) *Gy* are displayed; $(x, y, z)_{DICOM}$ - Cartesian system of DICOM coordinates with specified anatomical directions.

Legend to Figure 10. Local dose difference quotients towards the ipsilateral lacrimal gland (organ at risk OAR_i) for the stereotactic radiotherapy of the choroidal melanoma in patient no. 4 specified in Subsection 3.9. The scale for the representation of the dose difference quotients is 15.0 *mm*/(1 *Gy*/*mm*). $\Delta D/\Delta r\ (OAR_i)|_{20\%}^{95\%} = f(\varphi, \vartheta)$ - dose difference quotient as dose gradient vector linearised along the radius *r* and as a function of the azimuth φ and polar distance angle ϑ; for the three curvilinear coordinates, see Subsection 2.2; *V* - volume; *PTV* - planning target volume; D_1 = 95%, D_2 = 20% - levels of the proximal and distal isodoses of interest, respectively, relative to the nominal tumour dose 50 *Gy*; $(x, y, z)_{DICOM}$ - DICOM coordinates with the anatomical directions given in Figure 9.

to those in Table 1 indicate a successful optimisation of the beam geometry to achieve isodoses with best possible ball shape. Hence, the dose gradient problems in the irradiation series for the 13 brain metastases are almost isotropic.

On the other hand, the large values of E in Table 1 demonstrate that the dose gradient distributions in the irradiation series for the 25 ocular tumours are exceptionally anisotropic. In addition, the mean values of the locally defined *SADG* towards the organs at risk are 1.2 to 1.7 times smaller than the mean value of the globally defined *SADG* as shown in Table 2 and Figure 4.

The generation of locally steep dose gradients towards organs at risk with photon beams entails isodose surfaces that are more "ellipsoidal" than the associated planning target volumes. The enlargement of E of the isodoses of interest with a decreasing dose level was a substantial feature of the dose distributions in the irradiation series for the 25 choroidal melanomas and for the 13 brain metastases considered in [11, 18, 19]; an exemplary case is presented in Figure 9.

4.2. Quality of one-dimensional dose gradient indices

From all of the one-dimensional dose gradient indices, the approximated $SADG^*|_{D_2}^{D_1}$ was superior to the common dose gradient indices regarding the maximal errors relative to the $SADG(NT)|_{D_2}^{D_1}$ and the strongest correlation on the $SADG(NT)|_{D_2}^{D_1}$; for the underlying results, see Table 1 and Figure 3. The correctness of the mathematical approach to model the surfaces of the isodoses of interest in anisotropic dose gradient problems using ellipsoids as described in [15] was reinforced by the aforementioned results.

The $SADG^*|_{D_2}^{D_1}$ is the only explicit dose gradient index that makes it easy to interpret clinical values. Contrary to this, the application of implicit dose gradient measures makes it difficult for users to interpret the clinical values and to infer the physical dose gradients from the results [11].

4.3. Loss of accuracy due to discretisation

A measure for quantifying the discretisation level of a dose gradient problem includes the sample size of the dose gradient values taken into consideration in calculating a mean value of the dose gradients. The error in the $SADG_{RD}$ relative to the *SADG* is an indicator of the loss of accuracy due to discretisation. The *SADG* was determined on a low discretisation level using isodoses converted to structures with high local resolution. Otherwise, the calculation of the $SADG_{RD}$ is based on the dose matrix with a lower local resolution that is defined by a lattice parameter of 0.98 *mm*.

The error range in the $SADG_{RD}$ and the reduction factor of the average sample size given in the penultimate paragraph of Subsection 3.3 were 44.5% and 1/4.1, respectively. On the other hand, the author found an error range of 19.9% and a reduction factor of 1/1.3 in an irradiation series for 13 globular brain metastases [18]. Both pairs of values are quite different. Consequently, the smaller the sample size of a dose gradient problem, the greater the loss of accuracy of a more-dimensional dose gradient measure due to discretisation.

4.4. Loss of accuracy due to linearisation

The loss of accuracy due to the linearisation of the dose gradients by the difference quotients is demonstrated in the values of the errors in the $SADG_{RD}$ relative to the $VADG_{proj}$ as shown in Table 1. The $SADG_{RD}$ is a two-dimensional and the $VADG_{proj}$ is a three-dimensional dose gradient measure; both are determined using the dose matrix with the result that the discretisation levels are equal.

The error range in the $SADG_{RD}$ and the reduction factor of the average sample size given in the last paragraph of Subsection 3.3 were 18.5% and 1/10.5, respectively. On the other hand, the author found an error range of 5.2% and a reduction factor of 1/5.0 in an irradiation series for 13 globular brain metastases [19]. Both pairs of values are again quite different. Consequently, the smaller the sample size of the dose gradient values, the greater the loss of accuracy of a more-dimensional dose gradient measure due to linearisation.

The influence of the linearization along the third coordinate *r* on the values of the $SADG(NT)|_{D_2}^{D_1}$ is also visible in the results given in the third to last paragraph of Subsection 3.3. The two-dimensional $SADG(NT)|_{D_2}^{D_1}$ strongly depended on the levels D_1 and D_2 of the chosen isodoses of interest. The absolute values of the minimum, maximum, and median for the dose levels D_1 = 86% and D_2 = 43% were one and a half times larger than the corresponding values with D_1 = 95% and D_2 = 20%.

The differences in the values of the $SADG(NT)|_{D_2}^{D_1}$ arise from the transverse profile form of the intensity in a photon beam: The steepest dose fall-off occurs within the physical penumbra defined between the intensity levels 80% and 20% relative to the central axis intensity. Accordingly, the first dose level pair is located almost entirely inside the penumbra zone with the effect that the dose gradients were steeper than those between the isodoses of interest at the levels 95% and 20%. Moreover, clinical results of an irradiation series for 13 brain metastases proved a distinctly diminishing steepness of the dose fall-off on a decreasing dose level as shown with the dose-dependent dose gradient function defined in [19].

Please note: The loss of accuracy due to discretisation is more than twice the loss of accuracy due to linearization along one coordinate in space. In other words, the reduction of the discretisation level of a dose gradient problem is more fatal regarding the accuracy of its description than the simplification of a dose gradient measure by neglecting one dimension.

4.5. Correlation analyses between globally defined dose gradient measures

The correlations of all of the examined dose gradient measures on the $SADG(NT)|_{D_2}^{D_1}$ were statistically significant with $p \leq 0.010$, with exception of the correlation of the *DGI* with $p = 0.556$. Generally speaking, the explicit and inversely proportional dose gradient measures exhibited stronger correlations on the $SADG(NT)|_{D_2}^{D_1}$ than the implicit ones as shown in Figure 3.

The dose gradient indices *GI*, *DG*, *mGI*, and *DGI* showed false positive trends on an increasing value of the $SADG(NT)|_{D_2}^{D_1}$ in Figure 2. The author found the same trends of these dose gradient indices in an irradiation series for 13 brain metastases [11, 18, 19]. This severe deficiency of the aforementioned dose gradient indices has serious consequences: Users overestimate dose gradients and indifferent values of the dose gradient index can occur even though the physical dose gradients considerably vary. Effectively, such dose gradient indices do not allow direct or approximate comparisons between different patients, irradiation series, treatment techniques, and irradiation modalities concerning the dose gradients [11].

In principle, developers of dose gradient measures should avoid the occurrence of false characteristics by means of appropriate definitions and thorough examinations of the favoured measures. False trends in dose gradient measures can deeply unsettle users with the aforementioned serious difficulties.

The "bad" values of $r = -0.124$ and $p = 0.556$ with respect to the strength of correlation for the *DGI* on the $SADG(NT)|_{D_2}^{D_1}$ confirmed the intention of its authors to evaluate dose gradients without comparisons of multiple treatment plans [12].

4.6. Need for anisotropic dose gradient measures

The results summarised in Tables 1 and 2, as well as Figure 4 were evidence of the fact that the dose gradient problems in the chosen irradiation series for 25 choroidal melanomas have a high degree of anisotropy. Even more-dimensional dose gradient measures are not capable of adequately describing such dose gradient problems. Correspondingly, the correlations of all of the globally defined dose gradient measures on the locally defined $SADG(OAR_i)|_{D_2}^{D_1}$ towards the ipsilateral lacrimal gland were weak with $|r| \leq 0.404$. Exclusively, the correlations of the two-dimensional dose gradient measures $SADG(NT)|_{D_2}^{D_1}$ and $\overline{\Delta r}_{\Delta D}(NT)|_{D_2}^{D_1}$ were statistically significant with $p \leq 0.050$. These results highlighted the demand for anisotropic dose gradient measures that solely are able to describe local dose gradients towards critical structures.

More-dimensional dose gradient measures could also be needed in particle therapy because of the physically given differing dose gradients at the proximal and distal Bragg peak as well as in the lateral directions as a result of particle scattering. Considering the high dose level within a range of 40 to 80% relative to the Bragg peak maximum dose in the entry pathway[1], a flexible definition of the utilised dose gradient measures regarding the directions and levels of the isodose of interest would also be desirable.

[1]The relative dose values should be understood as examples for the dose levels in the plateau region of particle beams. The relative dose levels 40% and 80% are valid for an unmodulated 235 MeV proton beam and for a modulated proton beam with the same practical range, respectively.

4.7. Correlation analyses between dose gradients and dose-volume metrics

Five of the choroidal melanoma cases were not considered in Figures 7 and 8 because the superficially averaged distances of the related lacrimal glands were outside of the regarded distance classes: $\overline{a}_{PTV-OAR_i} \leq 5\ mm$ in two cases and $\overline{a}_{PTV-OAR_i} > 15\ mm$ in three cases. Correlation analyses with such small sample sizes would yield no reliable statements.

Another five cases were not considered in Figure 7 due to extremal values in the dose-volume metric $V_{10\,Gy}(OAR_i) \in [0, 100]\%$, which in turn indicated two little gaps and three large distances, respectively, between the planning target volumes and the related lacrimal glands. For the reason for neglecting these five cases in the correlation analyses, see the first paragraph.

Perceptible differences in the values of the dose-volume metric $V_{10\,Gy}(NT)$ were described in Subsection 3.5. Rounding errors were responsible for the discrepancies because the dose-volume metric was determined in two different ways within the utilised treatment planning system. Results out of dose-volume histograms are less accurate than voxel-based volume calculations of an isodose of interest, for what dose objects are created, due to the binning of dose values into discrete classes. Nevertheless, the author used the inaccurate values of $V_{10\,Gy}$ for the nonspecific normal tissue and organs at risk (OAR_i) for the correlation analyses in Subsection 3.7 because $V_{10\,Gy}(OAR_i)$ can solely be extracted from dose-volume histograms. The uniform database ensures comparability between the correlation results.

The strengths of the correlations for the optic nerve and papilla shown in Table 3 were lowest because of small ranges of variation in a_{min} and D_{max}; twelve (48%) of the 25 choroidal melanomas were located directly next to the papillae.

4.8. Correlations between local dose gradients and complication rates

The examined dose-volume metrics that specify the dose exposure of the nonspecific normal tissue as well as organs at risk showed strong and statistically significant correlations on the globally defined $SADG(NT)|_{D_2}^{D_1}$ and locally defined $SADG(OAR_i)|_{D_2}^{D_1}$, respectively.

On the other hand, relationships between these dose-volume metrics and treatment complication rates are well-known for many tissue types; dose-dependent complication probabilities can be predicted. In the simplest form, the relationships are dose tolerances of normal tissue to therapeutic irradiation, for instance, $TD_{5/5}$ (5% morbidity rate within five years) or $TD_{50/5}$ (50% morbidity rate within five years), for one third, two thirds, and the whole organ.

With this causal chain, the author found strong correlations of the treatment complication probabilities in the ipsilateral eyeball on the locally defined $SADG(OAR_i)|_{D_2}^{D_1}$. The final results of the present work are given in Tables 3 and 4; Table 4 is a convenient look-up table for clinical use: Medical physicists and radiation oncologists will be able to predict ocular toxicities dependent on the local dose gradients towards the ipsilateral lacrimal gland.

The author highlighted the lacrimal gland in the present work because of its fundamental importance in the eye-preserving radiotherapy of ocular tumours. If a lacrimal gland wholly or partially stops the secretion of tear fluid in consequence of radiation damage, the treated eye can cause chronic pains against which artificial tear supplement would not help; a further severe side effect is corneal opacity. The surgical excision of the eyeball out of its Tenon's capsule may be necessary to make the concerned patient free of pain – an eye loss should be avoided in all circumstances.

The current research findings are not surprising because precise calculations of local dose gradients towards adjacent organs at risk should enable clear distinctions in the degree of severity of treatment complications. The rationale is the knowledge that three-dimensional dose calculations with appropriate algorithms also yield exact values of dose-volume metrics for the normal tissue and organs at risk. These dose-volume metrics in turn allow for reliable predictions of treatment complication probabilities. Appropriate algorithms are, for instance, based on the Monte Carlo method or the explicit solution of the linearised Boltzmann transport equation.

4.9. Outlook and vision

The author presented relationships between the incidence of ocular toxicities and the locally defined

$SADG(OAR_i)|_{D_2}^{D_1}$ towards the ipsilateral lacrimal gland dependent on the distance between the planning target volume and the organ at risk.

The aforementioned procedure to obtain these relationships should be applied to all further organs at risk and to other tumour entities; while doing so, the substitution of the $SADG(OAR_i)|_{D_2}^{D_1}$ by the $VADG_{proj}(OAR_i)|_{D_2}^{D_1}$ defined in [19] should be kept in mind. Moreover, the discovered relationships have to be secured through clinically conducted validations.

The *SADG* and $VADG_{proj}$ could be optimisation variables in intensity-modulated radiotherapy (IMRT), arc therapy (IMAT), and proton therapy (IMPT). One or both gradient measures could replace all of the dose conditions and dose constraints for the organs at risk during the optimisation process. The rationale is that an irradiation unit does not deliver organ doses but dose profiles with well-known penumbras that specify the dose fall-off at the edges of an irradiation field.

5. CONCLUSION

The *SADG* is an explicit and two-dimensional description of dose gradient problems that exactly quantifies anisotropic dose gradient distributions – globally and locally. Explicit dose gradient measures make it easy to compare and correctly interpret results with respect to the quality of dose gradients – contrary to implicit dose gradient indices. The values of the globally and locally defined *SADG* were quite different in the irradiation series for 25 choroidal melanomas. This circumstance reinforced the need of multi-dimensional dose gradient measures.

In addition, dose gradient distributions in particle therapy are *per se* anisotropic because of the physically given differing dose gradients in the proximal, distal, and lateral directions related to the source and central axis of a particle beam. Treatment planning in particle therapy seems to be a typical application field for anisotropic dose gradient measures.

The approximated $SADG^*$, calculable within seconds, showed the smallest relative errors and strongest correlations on the globally defined *SADG* at the boundary of irregularly formed target volumes of all of the examined one-dimensional dose gradient indices. In this context, the reduction of the discretisation level of a dose gradient problem is more fatal regarding the accuracy of its description than the simplification of a dose gradient measure by neglecting one dimension.

Just like exact three-dimensional dose calculations with the values of dose-volume metrics for normal tissue and organs at risk allow for reliable predictions of radiogenic normal tissue complications and organ toxicities, the *SADG* should be able to do this. The author presented a natural correlation of the incidences of ocular toxicities on the locally defined *SADG* towards the ipsilateral lacrimal gland. The capability of the *SADG* concerning the quantification of local dose gradients that were fed into Table 4 is an important contribution to the eye-preserving radiotherapy of ocular tumours.

Each designer and user of dose gradient measures seeks such natural correlations to fulfil one important aim of ICRU Report no. 91 that is to better associate treatment complications with the values of dose gradient indices *via* rigorous and uniform reporting of these parameters.

The novel relative ellipsoidality E was defined in Eq. (3) to quantify the irregularity of surfaces and volumes of interest in contrast to an ideal spherical shape. It helps optimising beam geometry to achieve isodoses with the best possible ball shape, for instance, if lesions are embedded in homogeneous normal tissue. Additionally, E is a measure of the anisotropy of dose gradient distributions. The author showed that the present irradiation series covers exceptionally anisotropic dose gradient problems.

FUNDING

No funding at all has been claimed for this study.

ACKNOWLEDGEMENT

The author thanks Professor Ilja Frank Ciernik, head of department, for the provision of the utilised treatment planning system.

CONFLICT OF INTEREST STATEMENT

Markus Wösle declares that he has no competing interest.

APPENDIX

A.1. Definitions of common dose gradient measures

The definitions of the common dose gradient indices are summarised and explained in detail in Appendix A.1 of [18]; the advanced dose gradient index *aGI* is the subject of [11]. Appendices A.2 and A.3 deal with the two-dimensional dose gradient measures. Finally, the three-dimensional dose gradient measure $VADG_{proj}$ is the key issue of [19].

For all of the dose gradient measures discussed in the present study, the formula symbols, basic features like unit, dimensionality, and mathematical category, as well as the referring references are listed in Table A.1.

A.2. Superficially averaged dose gradient

The mathematical formulations of the linearised two-dimensional anisotropic dose gradient problem for nonspecific normal tissue (*NT*) and an arbitrary organ at risk (OAR_i)

$$SADG(X)|_{D_2}^{D_1} = \frac{1}{\Omega_X} \cdot \int_{(\varphi_X)} \int_{(\vartheta_X)} \frac{D_2 - D_1}{r_2(\varphi,\vartheta) - r_1(\varphi,\vartheta)} \cdot \sin\vartheta \cdot d\vartheta \cdot d\varphi \in \mathbb{R}^-, \quad X \in \{NT, OAR_i\} \qquad \text{(A.1)}$$

are quotients of surface integrals of the dose difference quotient $\Delta D/\Delta r$ and solid angles. The underlying system of coordinates K= $\{O, r, \varphi, \vartheta\}$ is defined by the origin *O* in the geometrical mass centre of the planning target volume and three curvilinear coordinates: radius *r*, azimuth φ, and polar distance angle ϑ. Eq. (A.1) is the result of applying the generalised first mean value theorem for integration [21] to the surface integrals.

The anisotropic radii r_1 and r_2 are the lengths of the position vectors to the surface points of the isodoses of interest. Their dose levels D_1 and D_2 define the surfaces of the treated and irradiated volumes, respectively. The surface element and solid angle element of the unit sphere are $dS \equiv d\Omega = \sin\vartheta \cdot d\vartheta \cdot d\varphi$ with which the dose difference quotient must be integrated. For the normal tissue, the integration range is the entire solid angle $\Omega_{NT} = 4 \cdot \pi\ sr$ with the angle ranges $\varphi_{NT}=[0, 2 \cdot \pi]$ and $\vartheta_{NT}= [0, \pi]$. For each organ at risk, the individual segment Ω_{OAR_i} of the entire solid angle is defined by the angle ranges φ_{OAR_i} and ϑ_{OAR_i}; for details see Eqs. (8) and (9) as well as [18].

All of the needed input data are content of the structure file `RS.*.dcm` from the utilised treatment planning system. The *SADG* values can also be calculated using the dose matrix in the dose file `RD.*.dcm` from the utilised treatment planning system. For distinctiveness of the basic input data, the quantity $SADG_{RD}$ receives the input file type as a subscript [18].

A.3 Superficially averaged radius difference

The superficially averaged radius difference

$$\overline{\Delta r}_{\Delta D}(X)|_{D_2}^{D_1} = \frac{D_2 - D_1}{SADG(X)|_{D_2}^{D_1}} \in \mathbb{R}^+, \quad X \in \{NT, OAR_i\} \qquad \text{(A.2)}$$

is a result of applying the definition of the dose difference quotient $\Delta D/\Delta r = (D_2 - D_1)/(\overline{r_2 - r_1})$ on the results of Eq. (A.1); it is itself a dose gradient measure [18].

A.4. Geometrical flattening of celestial bodies

Celestial bodies that rotate around its own axis exhibit geometrical flattenings at the two poles due to plastic deformations caused through centrifugal, gravitational, and restoring forces of the deformations. The surfaces of such bodies can be mathematically modelled by means of a rotational ellipsoid in good approximation. The semi-major axes $a \equiv b$ in the equatorial plane are identical, and the perpendicular semi-minor axis $c < a$ differs from them. The resulting geometrical flattening is defined as

$$A_{geo} = \frac{a - c}{a} > 0. \qquad \text{(A.3)}$$

The results are usually specified as proper fractions. For example, the geometrical flattening of the planet Earth is $A_{geo} \approx 1/298.2$ [25].

A.5. Study results about ocular toxicities

Batth *et al.* performed a study enclosing 40 consecutive patients with head and neck cancer and with involvement of the nasal cavity or paranasal sinuses that were treated by means of intensity-modulated radiotherapy. The median of the prescribed dose was 66.0 *Gy* (range of 30.6 to 70.0 *Gy*); the median dose per fraction was 2.0 *Gy* (range of 1.8 to 2.1 *Gy*). The treatment planning system Hi-ART® and the dose delivery system TomoTherapy® (both: Accuray, Inc., Sunnyvale, CA, USA) were utilised [22].

Acute and late ocular toxicities were retrospectively graded according to the radiation toxicity criteria of the Radiation Therapy Oncology Group (RTOG) and the European Organisation for Research and Treatment of Cancer (EORTG) [26]. This rating is based on the degree of conjunctivitis, keratitis, corneal ulceration, retinopathy, retinal detachment or visual loss [22].

The authors performed ordinal logistic regression to characterise the relationship between the dose in the ipsilateral lacrimal gland and acute ocular toxicities. On the other hand, the effect of the dose in the regarded organ at risk on late ocular toxicities was characterised by logistic regression. The statistical results were significant for the correlations of ocular toxicities on a number of dose-volume metrics in the lacrimal gland: mean dose, maximum dose, $V_{10\,Gy}$, $V_{20\,Gy}$, and $V_{30\,Gy}$. The decisive results that will be utilised in the present work are summarised in the first three columns of Table A.2.

Table A.1. Characteristic features and primary references of 17 dose gradient measures. $X \in \{NT, OAR_i\}$ - arguments of the more-dimensional dose gradient measures are nonspecific normal tissue NT or any organ at risk OAR_i.

Dose gradient measure	Formula symbol	Unit	Dimensionality	Category[a]	Reference
Holistic conformity/gradient index, second component	CGI_g	1	1	Implicit	[16]
Volume of normal tissue receiving at least the dose D	$V_D(NT)$[b]	cm^3	1	Implicit	[6, 7]
Dose gradient index	GI	1	1	Implicit	[5]
Unified dosimetry index, fourth component	DG	1	1	Implicit	[17]
Volume ratio	VR	1	1	Implicit	[8]
Quality index	$f_{12\ Gy}$	1	1	Implicit	[10]
Modified dose gradient index	mGI	1	1	Implicit	[9]
Dose gradient index	DGI	1	1	Implicit	[12]
One-dimensional metric	$\Delta R_{1/2}$	mm	1	Reciprocal	[13]
Dose-dependent dose gradient index	$DGI(D)$	mm	1	Reciprocal	[14]
Spatially averaged radius difference	$\Delta r^*_{\Delta D}$	mm	1	Reciprocal	[15]
Spatially averaged dose gradient	$SADG^*\|_{D_2}^{D_1}$	Gy/mm[c]	1	Explicit	[15, 18]
Superficially averaged radius difference	$\overline{\Delta r}_{\Delta D}(X)$	mm	1, 2[d]	Reciprocal	[18]
Superficially averaged dose gradient	$SADG(X)\|_{D_2}^{D_1}$	Gy/mm[c]	1, 2[d]	Explicit	[18]
Superficially averaged dose gradient calculated with the dose matrix `RD.*.dcm`	$SADG_{RD}(X)\|_{D_2}^{D_1}$	Gy/mm[c]	1, 2[d]	Explicit	[18]

Table A.1 continued.

Volumetrically averaged dose gradient	$VADG_{proj}(X)\|_{D_2}^{D_1}$	*Gy*/*mm*[c]	1, 3[d]	Explicit	[19]
Advanced dose gradient index	*aGI*	*cm*	1	Implicit[e]	[11]

[a]Mathematical classification scheme according to [18]. [b]For instance, D = 12 *Gy* for healthy brain tissue. [c]Or %/*mm* (% – percent by dose). [d]1, in case of using the mean value. [e]Acts like a reciprocal dose gradient index.

Table A.2. Incidences of acute and late ocular toxicities of grade 2 or higher dependent on the mean dose in the lacrimal gland that can occur after the intensity-modulated radiotherapy for sinonasal tumours [22]; grading according to the radiation toxicity criteria of [26]. D_{mean} - mean dose in the organ at risk; TD_{hypo} - tolerance dose for the hypofractionation according to Eq. (12).

D_{mean} [*Gy*]	Incidence of acute toxicity [%]	Incidence of late toxicity [%]	TD_{hypo} (D_{mean}) [*Gy*]
∈[1.0, 5.0[	0.0	0.0	∈[1.5, 6.0[
∈[5.0, 15.0[	12.5	12.5	∈[6.0, 13.3[
∈[15.0, 25.0[	57.1	28.6	∈[13.3, 18.6[
∈[25.0, 35.0[	80.0	60.0	∈[18.6, 23.0[
≥ 35.0	100.0	100.0	≥ 23.0

REFERENCES

1. Landberg, T., Chavaudra, J., Dobbs, J., Gerard, J. P., Hanks, G., Horiot, J. C., Johansson, K. A., Möller, T., Purdy, J., Suntharalingam, N. and Svensson, H. 1999, J. Int. Comm. Radiat. Units Meas., 32, 1.
2. International Commission on Radiation Units and Measurements. 2010, J. Int. Comm. Radiat. Units Meas., 10, 1.
3. International Commission on Radiation Units and Measurements. 2014, J. Int. Comm. Radiat. Units Meas., 14, 1.
4. Paddick, I. 2000, J. Neurosurg., (Suppl. 3), 93, 219.
5. Paddick, I. and Lippitz, B. 2006, J. Neurosurg. (Suppl.), 105, 194.
6. Flickinger, J. C., Kondziolka, D., Lunsford, L. D., Kassam, A., Phuong, L. K., Liščák, R. and Pollock, B. 2000, Int. J. Radiat. Oncol. Biol. Phys., 46, 1143.
7. Korytko, T., Radivoyevitch, T., Colussi, V., Wessels, B. W., Pillai, R., Maciunas, R. J. and Einstein, D. B. 2006, Int. J. Radiat. Oncol. Biol. Phys., 64, 419.
8. Liščák, R., Novotný, J,. Urgošik, D., Vladyka, V. and Šimonová, G. 2000, Radiosurgery, 3, 205.
9. Ohtakara, K., Hayashi, S. and Hoshi, H. 2011, J. Radiat. Res., 52, 592.
10. Hellerbach, A., Luyken, K., Hoevels, M., Gierich, A., Rueß, D., Baus, W. W., Kocher, M., Ruge, M. I. and Treuer, H. 2017, Radiation Oncology, 12, 136.
11. Wösle, M. 2021, Trends in Cancer Research, 16, 55.
12. Sheth, N. S., Sim, S., Cheng, J., Lustgarten, J., Estin, D., Olson, T., Weiss, M., Murphy, S., Chen, Y. and Yang, J. 2011, Int. J. Radiat. Oncol. Biol. Phys., 81, S867.
13. Ruschin, M., Lee, Y., Beachey, D., Yeboah, C., Wronski, M., Babic, S., Lochray, F., Nico, A., Khan, L., Soliman, H. and Sahgal, A. 2016, Technology in Cancer Research and Treatment, 15, 130.
14. Sung, K. and Choi, Y. E. 2018, PLoS One, 13, e0196664.
15. Wösle, M., Krause, L., Sreenivasa, S., Vordermark, D. and Ciernik, I. F. 2018, Strahlenther. Onkol., 194, 929.
16. Wagner, T. H., Bova, F. J., Friedman, W. A., Buatti, J. M., Bouchet, L. G. and Meeks, S. L. 2003, Int. J. Radiat. Oncol. Biol. Phys., 57, 1141.

17. Akpati, H., Kim, C. S., Kim, B., Park, T. and Meek, A. 2008, Journal of Applied Clinical Medical Physics, 9, 99.
18. Wösle, M. 2020, Z. Med. Phys., 30, 70.
19. Wösle, M. 2021, Trends in Cancer Research, 16, 39.
20. Nikova, A. S., Ganchev, D., Birbilis, T. A., Sfyrlida, K. and Nakova, N. 2017, J. Radiol. Radiat. Ther., 5, 1076.
21. Bronstein, I. N. and Semendjajew, K. A. 1987, Taschenbuch der Mathematik, 23rd Ed., Verlag Harri Deutsch, Thun, Frankfurt (Main).
22. Batth, S. S., Sreeraman, R., Dienes, E., Beckett, L. A., Daly, M. E., Cui, J., Mathai, M., Purdy, J. A. and Chen, A. M. 2013, Br. J. Radiol., 86, 20130459.
23. Herrmann, T., Baumann, M. and Dörr, W. 2005, Klinische Strahlenbiologie – kurz und bündig, 4th Ed., Elsevier Urban & Fischer, München, Jena.
24. Weiß, C. 2001, Basiswissen Medizinische Statistik, 2nd Ed., Springer-Verlag GmbH, Berlin, Heidelberg, New York.
25. Demtröder, W. 2015, Experimentalphysik – Band 1: Mechanik und Wärme, 7th Ed., Springer Spektrum, Berlin, Heidelberg.
26. Cox, J. D., Stetz, J. and Pajak, T. F. 1995, Int. J. Radiat. Oncol. Biol. Phys., 31, 1341.